Rotatorlike gantry optics

M. Pavlovič,[1] M. T. F. Pivi,[2] I. Strašík,[2] V. Rizzoglio,[2] M. G. Pullia,[3] L. Adler,[2] G. Guidoboni,[2] C. Maderböck,[2] D. Prokopovich,[2] and G. Kowarik[4]

[1]*Slovak University of Technology in Bratislava, FEI STU, Ilkovičova 3, 84104 Bratislava, Slovakia*
[2]*EBG MedAustron, Marie-Curie-Straße 5, 2700 Wiener Neustadt, Austria*
[3]*CNAO Foundation, Str. Campeggi 53, 27100 Pavia, Italy*
[4]*GKMT Consulting e.U., Argentinierstraße 71, TOP12, 1040 Vienna, Austria*

(Received 19 April 2024; accepted 26 June 2024; published 26 July 2024)

Rotating gantries are commonly used in ion-therapy facilities to assist and support optimizing the dose distribution delivered to the patient. They are installed at the end of the beamlines and rotated mechanically in the treatment room. In synchrotron-based facilities, the gantries must be able to transport slowly extracted beams with essentially different emittance patterns in the two transverse planes. Such beams will be referred to as the asymmetric beams. A special device called rotator has been proposed as a possible solution. The worldwide first beamline with the rotator has been recently commissioned. The original rotator concept uses an "external" rotator that is a part (a module) of the beamline the gantry is connected to. In this paper, a novel gantry ion-optical concept integrating the rotator optics into the gantry optics is introduced. The first-order gantry transfer matrix satisfies the so-called sigma-matching ion-optical constraints, and—at the same time—it possesses the format of a rotator transfer matrix. The rotator-matching and the sigma-matching principles are combined in the gantry transfer matrix, which means that the sigma-matching gantry acts simultaneously as a rotator without the need for an extra rotator device. In addition, scattering in the gantry nozzle is used to balance the asymmetric beam emittances in the two transverse planes without an additional scattering foil. In this way, the presented ion-optical concept combines all three known matching techniques—the sigma matching, the rotator matching, and the scattering-foil matching—within the gantry beam transport system. Such a beam transport system provides the best matching result and full angular independence of the beam parameters at the gantry isocenter. It also makes it possible to optimize the beam parameters not only at the gantry isocenter but also at the beam monitors located in the gantry nozzle without increasing the number of gantry quadrupoles. There are two possible versions of such gantry optics: the point-to-point and the parallel-to-point optics. They both are presented in this paper. Theoretical calculations are supported by beam transport simulations performed with the WinAGILE code. Feasibility of the newly proposed ion-optical concept is demonstrated on the MedAustron proton gantry. However, it can be applied to any rotating gantry at any ion-therapy facility. The presented design is the first rotatorlike gantry ion-optical concept worldwide.

DOI: 10.1103/PhysRevAccelBeams.27.073502

I. INTRODUCTION

Ion therapy is an attractive cancer-treatment modality profiting from a favorable depth-dose profile of high-energy ion beams in an absorbing medium that is known as the Bragg curve or the Bragg peak. Proton therapy beams with kinetic energy up to ≈250 MeV are usually delivered by cyclotrons or synchrotrons. Ion-therapy beams, usually carbon beams with kinetic energy up to ≈400 MeV/n, are delivered by synchrotrons. These energies are too high for cyclotrons. Synchrotrons provide an additional advantage of active energy variation. On the other hand, the synchrotron-based facilities are larger, more expensive, and more complex than the cyclotron-based ones and bring some specific beam-transport challenges.

Ion-therapy beams delivered by a synchrotron have substantially different emittances and emittance diagrams in the two transverse planes. The reason for this asymmetry is the resonant slow extraction that takes place in the bending plane of the synchrotron [1–4]. The resonant slow extraction is used to obtain the beam spills suitable for pencil-beam scanning [5]. This practically means spills of modest intensity (typically $\approx 10^{10}$ and $\approx 10^{8}$ particles per spill for protons and carbon ions, respectively) lasting

typically few ($\approx 1 \div 15$) seconds. In case of the pencil-beam scanning, the beam parameters at the irradiation place (usually the gantry isocenter) are determined by the beam optics, which is different from the passive beam delivery techniques. The passive beam delivery techniques use scattering and collimation of the beam upstream of the patient [6]. The situation becomes more complicated when the pencil-beam scanning is incorporated into a rotating gantry [7,8]. The beam-spot asymmetry may have severe impact on the dose distribution especially on the edge of the irradiation field. For scanning carbon-ion-therapy facilities, such effects are reported when beam-spot asymmetry exceeds 15% [9]. Thus the transport of the asymmetric beams in rotating ion optical systems requires special care to remove dependence of the selected beam parameters at the irradiation place on the gantry rotation angle.

Several techniques have been developed to solve this challenge: (i) the emittance balancing with the aid of a scattering foil, (ii) the beam rotation at the gantry entrance using a special rotated matching section called a rotator, and (iii) the so-called sigma matching based on special ion-optical constraints imposed on the gantry transfer matrix. They are going to be explained and discussed below in a dedicated section.

Our ion-optical concept applies the rotator principle directly to the gantry optics without the need of using the rotator as a separate additional part (module) of the incoming fixed beamline. In other words, the gantry first-order transfer matrix satisfies the sigma-matching ion-optical constraints and—at the same time—it possesses the rotatorlike matrix format. This means that the gantry acts as a rotator. Such gantry optics will be referred to as the rotatorlike gantry optics. In addition, the beam transport in the gantry is combined with beam scattering in the gantry nozzle. Such a beam transport system provides the best matching result and full angular independence of the beam parameters at the gantry isocenter. It also makes it possible to optimize the beam parameters not only at the gantry isocenter but also at the beam monitors located in the gantry nozzle without increasing the number of gantry quadrupoles. The presented design is the first rotatorlike gantry ion-optical concept worldwide. Both the point-to-point, and the parallel-to-point rotatorlike gantry versions are presented in this paper.

II. BASIC DEFINITIONS AND MAIN ASSUMPTIONS

A. The coordinate systems

The transverse particle coordinates $(x, x' = \frac{dx}{ds}, z, z' = \frac{dz}{ds})$ are given in a local rectangular right-handed coordinate system $[x, s, z]$, where s is the longitudinal coordinate along the design orbit, $[x, s]$ stands for the ion-optical horizontal plane, and $[s, z]$ stands for the ion-optical vertical plane. The ion-optical horizontal plane is defined as the bending plane of the dipoles. There are two local coordinate systems. The local coordinate system of the incoming fixed beamline serving the beam to the gantry entrance and the local coordinate system of the gantry. The horizontal plane of the fixed beamline coincides with the bending plane of its dipoles. It is identical with the horizontal plane of a synchrotron, which is the plane of beam extraction. The gantry horizontal plane coincides with the bending plane of the gantry dipoles and bears no relation to the real gantry orientation in the absolute laboratory coordinate system. The local gantry coordinate system rotates together with the gantry. A coordinate system rotation appears between the fixed beamline exit and the gantry entrance. This coordinate system rotation (CSR) is described by the transfer matrix, $\mathbf{R_{CSR}}$:

$$\mathbf{R_{CSR}} = \begin{pmatrix} \cos\varphi & 0 & \sin\varphi & 0 \\ 0 & \cos\varphi & 0 & \sin\varphi \\ -\sin\varphi & 0 & \cos\varphi & 0 \\ 0 & -\sin\varphi & 0 & \cos\varphi \end{pmatrix}, \qquad (1)$$

where φ is the angle between the two local coordinates systems, anticlockwise rotation stands for the positive angles. It should be noted that the absolute gantry rotation angle is usually defined to be zero for the upright gantry position with the exit beam pointing downward. With this definition, $\varphi = 0°$ at the gantry rotation angle 90° when the gantry is lying horizontally, and its dipoles bend in the same plane as the synchrotron and the fixed beamline dipoles. In other words, at $\varphi = 0°$, the horizontal gantry plane receives the horizontal beam parameters from the fixed beamline, and the vertical gantry plane receives the vertical beam parameters from the fixed beamline. At $\varphi = 90°$, the situation is reversed. In this paper, we will always refer to the gantry rotation angle, φ, as the angle between the local coordinate system of the gantry and the local coordinate system of the incoming fixed beamline.

The other two particle coordinates, namely the longitudinal path difference and the relative momentum deviation are not relevant for the present work. Therefore, they will not be included in mathematical treatment. Thus the matrix formalism can be restricted to 4×4 matrices through this paper. In addition, it is also restricted to the first-order transfer matrices. Nevertheless, it must be emphasized that the 4×4 matrix formalism is enough for the: (i) theoretical analysis of the problem; (ii) description and explanation of the working principle of the ion-optical concept presented in the paper; (iii) deriving the corresponding ion-optical constraints imposed on the incoming fixed beamline and the gantry.

The beam transport calculations presented in this work have been performed with full 6×6 transfer matrices, which is an intrinsic property of the WinAGILE computer code used to perform the calculations (see also Sec. IV C).

B. The beam model

The beam at the fixed beamline exit is characterized by the beam sigma matrix, $\boldsymbol{\sigma}$:

$$\boldsymbol{\sigma} = \begin{pmatrix} \sigma_{11} & \sigma_{12} & 0 & 0 \\ \sigma_{12} & \sigma_{22} & 0 & 0 \\ 0 & 0 & \sigma_{33} & \sigma_{34} \\ 0 & 0 & \sigma_{34} & \sigma_{44} \end{pmatrix} = \begin{pmatrix} \langle xx \rangle & \langle xx' \rangle & 0 & 0 \\ \langle x'x \rangle & \langle x'x' \rangle & 0 & 0 \\ 0 & 0 & \langle zz \rangle & \langle zz' \rangle \\ 0 & 0 & \langle z'z \rangle & \langle z'z' \rangle \end{pmatrix} = \begin{pmatrix} \boldsymbol{\sigma}_{\mathbf{h}} & 0 \\ 0 & \boldsymbol{\sigma}_{\mathbf{v}} \end{pmatrix}, \quad (2)$$

where the terms of the sigma matrix represent the covariance of the quantities indicated in brackets. This model assumes no correlation between the horizontal and vertical planes in the incoming beam. This assumption can be converted into a constraint imposed on the fixed incoming beamline that must contain no beam transport elements causing horizontal-to-vertical coupling in particle motion. If the fixed beamline does contain a rotator, this is no longer true. However, the rotator is a rather specific ion-optical device (see Sec. III B for the basic explanation of the rotator optics) that violates this constraint only locally. A plausible interpretation in this case is considering that the fixed beamline ends at the coupling point to the rotator. Inside the rotator, in the local coordinate system of the rotator, the covariances are locally not zeros due to the coordinate system rotation at the rotator entrance. Nevertheless, they become zeros again at the gantry entrance thanks to the second coordinate system rotation at the rotator exit because the overall transfer matrix including both coordinate system rotations is not a function of the rotation angle.

In the beam sigma matrix according to Eq. (2), the transverse submatrices, $\boldsymbol{\sigma}_{\mathbf{h}}$ and $\boldsymbol{\sigma}_{\mathbf{v}}$, can be—in general—written in terms of the Twiss parameters β, α, γ, and the geometrical rms beam emittance, ε, as follows (e.g., in the horizontal plane):

$$\boldsymbol{\sigma}_{\mathbf{h}} = \varepsilon_h \begin{pmatrix} \beta_h & -\alpha_h \\ -\alpha_h & \gamma_h \end{pmatrix}, \quad (3)$$

$$\text{with} \quad \beta_h \gamma_h = 1 + \alpha_h^2 \quad \text{and} \quad \varepsilon_h = \sqrt{\|\boldsymbol{\sigma}_{\mathbf{h}}\|}. \quad (4)$$

Equations (3) and (4) hold in the ion-optical horizontal plane. Equivalent relations hold correspondingly in the ion-optical vertical plane, too. The asymmetric beam can be then defined as the beam with (essentially) different horizontal and vertical beam emittances:

$$\varepsilon_h \neq \varepsilon_v. \quad (5)$$

More specifically, the beam emittance in the plane of the slow beam extraction is typically much smaller ($\approx 1\%$) than the beam emittance in the vertical plane. However, the rotatorlike gantry optics presented in this paper works for any horizontal-to-vertical emittance ratio. There are also other differences between the horizontal and vertical beam characteristics that are described in Refs. [1–4]. In these references, the concept of the so-called bar-of-charge has been introduced. We have adopted this concept. We assume that at the fixed beamline exit, the vertical beam-emittance diagram is an ellipse with the rms geometrical emittance of the order of $\approx \pi$ mm mrad populated with beam particles following normal Gaussian distribution. We will refer to this kind of emittance diagram as "the full ellipse." In contrast to this, the bar-of-charge with $\varepsilon_h \ll \varepsilon_v$ (shortly "the bar") will be assumed in the horizontal plane of the fixed beamline. The bar profile may differ from the Gaussian distribution toward a more rectangular shape. The reason is that during the slow-extraction process from the synchrotron, the particles in the horizontal phase space lay on the separatrix, which is cut by the electrostatic septum. The distribution in the horizontal phase space shows, therefore, a sharp edge, at least on one side. Details on the thickness of the separatrix and on the particle distribution inside the bar are not critical in the presented ion-optical concept. Replacing the bar by the so-called unfilled (empty) ellipse as introduced in Refs. [2,3] is not followed in this work. The rotatorlike gantry optics makes it possible to avoid this approach.

C. The gantry transfer matrix and matrix transformations

The gantry optics is described by its first-order transfer matrix taken from the gantry entrance to the gantry isocenter in the local gantry coordinate system, $\mathbf{R}_{\mathbf{GAN}}$:

$$\mathbf{R}_{\mathbf{GAN}} = \begin{pmatrix} g_{11} & g_{12} & 0 & 0 \\ g_{21} & g_{22} & 0 & 0 \\ 0 & 0 & g_{33} & g_{34} \\ 0 & 0 & g_{43} & g_{44} \end{pmatrix}. \quad (6)$$

Similar to the incoming fixed beamline, no coupling between the horizontal and vertical planes is assumed in the gantry optics. The gantry is assumed to be fully achromatic, i.e., the dispersion function, D, and its derivatives, $D' = \frac{dD}{ds}$, at the gantry isocenter are assumed to be zero. While this is automatically fulfilled in the vertical gantry plane (the nonbending plane of the gantry dipoles), it requires two ion-optical constraints, $D_x = 0$ and $D'_x = 0$ in the horizontal gantry plane. It should be noted that the incoming fixed beamline is assumed to be fully achromatic in both transverse planes, too. This means that the gantry

optics must be a closed dispersion "bump" from the gantry entrance to the gantry isocenter in the horizontal plane.

Let us define two gantry versions according to the imaging mode. The point-to-point imaging gantry optics is characterized by $g_{12} = g_{34} = 0$. The parallel-to-point imaging gantry optics is characterized by $g_{11} = g_{33} = 0$.

The overall transformation of the beam sigma matrix from the fixed beamline exit, $\boldsymbol{\sigma}$, to the beam sigma matrix at the gantry isocenter, Σ, reads

$$\Sigma = (\mathbf{R_{GAN}} \times \mathbf{R_{CSR}}) \times \boldsymbol{\sigma} \times (\mathbf{R_{GAN}} \times \mathbf{R_{CSR}})^{\mathrm{T}}. \quad (7)$$

III. A BREIF OVERVIEW OF THE EXISTING MATCHING TECHNIQUES

Several matching techniques for transport of asymmetric beams in rotating gantries have been developed [10]. They can be classified into three main categories. Each category represents a different working principle and can be represented by one typical method. Because the rotatorlike gantry optics is a combination of the main existing matching techniques, it is necessary to describe them first.

A. The scattering foil

This technique removes the emittance asymmetry upstream of the gantry entrance by inserting a dedicated scattering foil into the beam. The underlying description of the scattering-foil matching is the quadratic sum of the beam divergence before the scatterer, δ_0, and the scattering contribution, $\delta_{\mathrm{scatter}}$, yielding the beam divergence after the scatterer, $\delta_{\mathrm{total}} = \sqrt{\delta_0^2 + \delta_{\mathrm{scatter}}^2}$. In addition to this, the corresponding emittance blowup can be further optimized by proper orientation of the emittance patterns in the phase space. The beam on the foil shall be shaped in such a way that its emittance diagram in the low-emittance plane (usually the horizontal one) is "flat" in the phase space (large beam size, small beam divergence), whereas the emittance diagram in the large-emittance plane is "upright" in the phase space (small beam size and large beam divergence). Under these circumstances, the emittance blowup due to the scattering is larger in the low-emittance plane compared to the large-emittance one. The horizontal and vertical emittances get approximately balanced. The energy dependence of the scattering is compensated for by the foil rotation. High-energy beams enter the foil nonperpendicular to its surface and traverse an effectively thicker foil. More details concerning this technique can be found in Ref. [11]. It is employed for example at the Heavy Ion Medical Accelerator in Chiba, Japan, superconducting heavy-ion gantry [12–15].

It should be emphasized that our design utilizes the principle of the scattering-foillike matching, but there is no dedicated scattering foil used. Thus, our design reduces the amount of matter traversed by the beam down to theoretical minimum. It uses scattering in the gantry nozzle merely from the components that must be inevitably there for other purposes, like the vacuum window and the beam monitors. The scattering is optimized with the aid of proper adjustment of the beam parameters at the vacuum window.

B. The rotator matching

The rotator matching tolerates the emittance asymmetry at the gantry entrance but makes it independent from the gantry rotation angle. The beam at the gantry entrance is rotated together with the gantry, which is achieved with the aid of a dedicated device—the so-called rotator—that is a part (a module) of the incoming fixed beamline. In general, the rotator is a double-achromatic ion-optical system characterized by the special format of its transfer matrix:

$$\mathbf{R_{ROT}} = \begin{pmatrix} r_{11} & r_{12} & 0 & 0 \\ r_{21} & r_{22} & 0 & 0 \\ 0 & 0 & -r_{11} & -r_{12} \\ 0 & 0 & -r_{21} & -r_{22} \end{pmatrix}, \quad (8)$$

where $\mathbf{R_{ROT}}$ is the first-order transfer matrix from the rotator entrance to the rotator exit in its local coordinate system. When such an ion-optical system is placed in-between the fixed beamline exit and the gantry entrance, and physically rotated with respect to the fixed beamline by half of the gantry angle, the gantry rotation is subdivided into two coordinate-system rotations. The first one appears between the beamline exit and the rotator entrance, and the second one appears between the rotator exit and the gantry entrance, each by half of the gantry angle. The overall transfer matrix, $\mathbf{R_{TOTAL}}$, from the fixed beamline exit to the gantry entrance reads:

$$\mathbf{R_{TOTAL}} = \begin{pmatrix} \cos\frac{\varphi}{2} & 0 & \sin\frac{\varphi}{2} & 0 \\ 0 & \cos\frac{\varphi}{2} & 0 & \sin\frac{\varphi}{2} \\ -\sin\frac{\varphi}{2} & 0 & \cos\frac{\varphi}{2} & 0 \\ 0 & -\sin\frac{\varphi}{2} & 0 & \cos\frac{\varphi}{2} \end{pmatrix} \times \mathbf{R_{ROT}} \times \begin{pmatrix} \cos\frac{\varphi}{2} & 0 & \sin\frac{\varphi}{2} & 0 \\ 0 & \cos\frac{\varphi}{2} & 0 & \sin\frac{\varphi}{2} \\ -\sin\frac{\varphi}{2} & 0 & \cos\frac{\varphi}{2} & 0 \\ 0 & -\sin\frac{\varphi}{2} & 0 & \cos\frac{\varphi}{2} \end{pmatrix}, \quad (9)$$

where φ is the gantry rotation angle as defined in Sec. II A. It can easily be shown by performing the above matrix multiplication that:

$$\mathbf{R_{TOTAL}} = \mathbf{R_{ROT}} \neq f(\varphi). \quad (10)$$

The transfer matrix from the fixed beamline exit to the gantry entrance is not a function of the gantry rotation

angle. Therefore, not only the beam but even all individual beam particles have the same coordinates at the gantry entrance independently from the gantry rotation angle. Thanks to this feature, the rotator also matches the dispersion function since a particle with a certain momentum deviation enters the gantry always at the same position and angle. In fact, the rotator was originally invented to match the dispersion function in chromatic gantries, e.g., the Riesenrad gantry [16,17]. In addition to this, each of the two gantry transverse planes receives the same input beam parameters at all gantry angles. This makes it possible to design the gantry optics in a custom-tailored way just for those input beam parameters, which simplifies the gantry-optics design and increases its flexibility.

The working principle of the rotator is known from the literature since almost three decades [2,3,18]. The original proposal appeared even earlier [19]. However, the only beamline in the world with a rotator structure, presently in operation, is installed at the MedAustron-therapy accelerator in Wiener Neustadt, Austria [20,21]. Although the rotator-matching principle is very attractive, the need for another mechanically rotated ion-optical system—e.g., a $\approx$ 10 m long rotator lattice containing seven quadrupoles—is a technical complication. Besides the need for extra space and costs, it brings some specific beam-alignment and orbit-correction issues [21]. The rotatorlike gantry optics overcomes this complication. It succeeds in matching the gantry transfer matrix to the rotator-matrix format, hence profiting from unique properties of the rotator matching without the need of an "external" rotator. The ion-optical action of the rotator is taken over by the gantry optics itself.

It should be noted that—in contrast to the previously described scattering-foil matching—the rotator matching does not aim at balancing the horizontal and vertical beam emittances, i.e., at removing the beam asymmetry. It only removes the angular dependence of the beam parameters at the gantry entrance because the phase space practically rotates with the gantry. The gantry still receives an asymmetric beam. The gantry optics must be designed specifically for the bar in one of the gantry transverse planes, and for the full ellipse in the perpendicular one to make the beam spot round at the gantry isocenter.

C. The sigma matching

The sigma matching tolerates the emittance asymmetry as well as its angular dependence at the gantry entrance. The matching is subdivided into the incoming fixed beamline and the gantry. In case of the point-to-point imaging mode, the incoming fixed beamline must serve the beam satisfying the constraint at the beamline exit:

$$\sigma_{11} = \sigma_{33} = \sigma_{11\equiv 33} = \sigma_{33\equiv 11}, \tag{11}$$

which is equivalent to the same rms beam size in the horizontal and vertical planes served at the gantry entrance by the incoming beamline. Let us recall that the incoming fixed beamline is also assumed to serve zero dispersion function and its derivatives. Notation $\sigma_{11\equiv 33}$ stands for the σ_{11} term identical to the σ_{33} term. Similarly, $\sigma_{33\equiv 11}$ stands for the σ_{33} term identical to the σ_{11} term. This notation is going to simplify and speedup some analytical calculations later.

The gantry transfer matrix from the gantry entrance to the gantry isocenter (in the local gantry coordinate system) must satisfy simultaneously:

$$g_{12} = g_{34} = 0 \quad \text{and} \quad |g_{11}| = |g_{33}| = M, \tag{12}$$

which is equivalent to the point-to-point imaging, and the same magnification, M, in both transverse gantry planes simultaneously. It has been shown in Refs. [22,23] that conditions (11) and (12) yield

$$\Sigma_{11} = \Sigma_{33} \neq f(\varphi) \quad \text{and} \quad \Sigma_{13} = 0 \neq f(\varphi), \tag{13}$$

where Σ_{ij} indicates a sigma-matrix term at the gantry isocenter. Equation (13) means having the same and rotationally independent rms beam size at the gantry isocenter in both gantry transverse planes. The second condition ($\Sigma_{13} = 0$) means that there is no correlation between the horizontal and vertical particle coordinates (x, z) at the gantry isocenter. This means that the beam spot is round (in terms of rms) and not a tilted ellipse with identical horizontal and vertical projections in real space.

In case of the parallel-to-point imaging mode, the incoming fixed beamline must serve the beam satisfying the constraint at the beamline exit:

$$\sigma_{22} = \sigma_{44} = \sigma_{22\equiv 44} = \sigma_{44\equiv 22}, \tag{14}$$

which is equivalent to the same rms beam divergence in the horizontal and vertical plane served at the gantry entrance by the incoming beamline. The gantry transfer matrix from the gantry entrance to the gantry isocenter (in the local gantry coordinate system) must satisfy simultaneously:

$$g_{11} = g_{33} = 0 \quad \text{and} \quad |g_{12}| = |g_{34}| = M^*, \tag{15}$$

which is equivalent to the parallel-to-point imaging, and the same magnification factor, M^*, in both gantry transverse planes simultaneously. Conditions (14) and (15) yield the same result as in the case of the point-to-point imaging mode given by Eq. (13).

The sigma matching has been adopted by several gantry designs and gantries in operation [22–30]. The minimum number of gantry quadrupoles needed for this matching technique is six [23], which corresponds to the number of ion-optical constraints imposed on the gantry transfer matrix given by Eq. (12) or Eq. (15) plus two constraints concerning the dispersion function, $D_x = 0$ and $D'_x = 0$ at the gantry isocenter in the horizontal plane.

IV. MATERIALS AND METHODS

A. The MedAustron proton gantry

In order to demonstrate feasibility of the rotatorlike gantry optics, all theoretical considerations presented in this paper are going to be applied to the MedAustron proton gantry. The rotatorlike gantry optics has been achieved with the existing gantry layout and hardware (including the magnet power supplies) merely by finding a proper setting of the gantry quadrupoles.

The MedAustron proton gantry is a barrellike normal-conducting isocentric gantry based on the Paul Scherrer Institute Villigen, Switzerland) "gantry 2" design [31,32]. It is equipped with a 2D pencil-beam scanning system located upstream of the last 90° gantry dipole. No passive scattering beam delivery system is used at MedAustron. A cut of the gantry beamline through its bending midplane (the horizontal plane of the gantry local coordinate system) is shown in Fig. 1.

The gantry beamline starts from the so-called coupling point, which is the place where the gantry is connected to the incoming fixed beamline serving the beam to the gantry. The coupling point is also the point where the mechanical rotation of the gantry takes place. The coupling point is followed by the first part of the gantry beamline that is an on axis entrance straight section hosting a quadrupole doublet. After passing this on axis straight section, the beam is bent off axis by the first 58° dipole, transported through another quadrupole doublet and bent again by the second 58° dipole. The two 58° dipoles are identical but bend the beam in opposite directions. They use an edge focusing of +12° at the entrance as well as at the exit of the magnet. Next part of the gantry beamline is an off axis straight section hosting a quadrupole triplet and the 2D pencil-beam scanning system consisting of two scanning dipoles, vertical and horizontal, located in the vertical and horizontal focal point of the last 90° gantry dipole, respectively. The position of the focal points of the last gantry dipole is adjusted by its edge focusing. Such a location of the scanning magnets provides quasiparallel scanning. The scanning field is 20 cm × 12 cm in the horizontal and vertical gantry planes, respectively. Finally, the beam exits the last gantry dipole perpendicular to the gantry mechanical axis and crosses this axis at the point that is called the gantry isocenter. Usually (but not necessarily), the isocenter is used as the place of irradiation. The part of the beamline between the exit of the last gantry dipole and the isocenter, the so-called gantry nozzle, is used for beam monitoring and safety purposes with the aid of a set of dedicated beam monitors indicated schematically in Fig. 1 as DDS—the dose delivery system. The configuration of the gantry nozzle can be found in Ref. [21]. There is also an air gap of about 75 cm from the last nozzle monitor to the isocenter. Further beam transport elements of the gantry beamline—three dual-plane correctors used for orbit correction and three SFX (scintillating fibers hodoscope) beam-profile and beam-position monitors with fiber-spacing of 1 mm—are indicated in Fig. 1, too. The MedAustron proton gantry can be rotated from $\varphi = -90°$ to $\varphi = +90°$.

The vacuum part of the gantry beamline is terminated by a double vacuum window located at the exit of the vacuum chamber of the last gantry dipole. The vacuum window consists of two identical pairs of aluminum and Hostaphan® Polyester foils. The thickness of the Al-foil and the Hostaphan® foil is 5 and 190 μm, respectively. There is an evacuated gap of 14 mm between the two Al-Hostaphan® vacuum windows. The role and contribution of the vacuum window to the beam scattering in the gantry nozzle is going to be discussed in Sec. VI C.

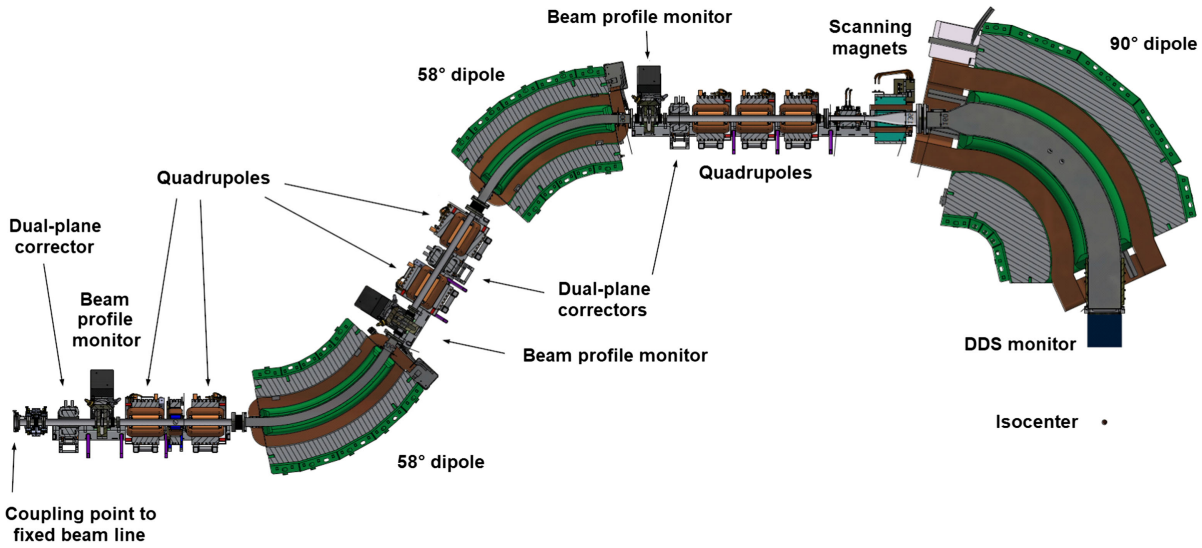

FIG. 1. Cut of the gantry beamline through its bending midplane. The beam enters the gantry from the left. DDS stands for the dose delivery system. The isocenter represents the virtual crossing point of the outcoming and (prolonged) incoming beam axes.

B. Matching of a rotator matrix

Matching of a rotator matrix can be effectively done using the following notation of the first-order transfer matrix of an ion-optical system based on the Twiss formalism (in one transverse plane) [33]:

$$\begin{pmatrix} \sqrt{\frac{\beta_1}{\beta_0}}(\cos\mu+\alpha_0\sin\mu) & \sqrt{\beta_0\beta_1}\sin\mu \\ \frac{\alpha_0-\alpha_1}{\sqrt{\beta_0\beta_1}}\cos\mu-\frac{1+\alpha_0\alpha_1}{\sqrt{\beta_0\beta_1}}\sin\mu & \sqrt{\frac{\beta_0}{\beta_1}}(\cos\mu-\alpha_1\sin\mu) \end{pmatrix}, \quad (16)$$

where β_0 and α_0 are the lattice functions at the entrance to the ion-optical system, β_1 and α_1 are the lattice functions at the exit from the ion-optical system, and μ is the phase advance. For matching purposes, without any loss of generality, one can set $\beta_0 = 1$ m and $\alpha_0 = 0$. The transfer matrix (16) simplifies to

$$\begin{pmatrix} \sqrt{\frac{\beta_1}{\beta_0}}\cos\mu & \sqrt{\beta_0\beta_1}\sin\mu \\ \frac{-\alpha_1}{\sqrt{\beta_0\beta_1}}\cos\mu-\frac{1}{\sqrt{\beta_0\beta_1}}\sin\mu & \sqrt{\frac{1m}{\beta_1}}(\cos\mu-\alpha_1\sin\mu) \end{pmatrix}. \quad (17)$$

Desired values of its terms are obtained by matching the output beta, alpha, and the phase advance. For example, the point-to-point imaging mode is achieved with the phase-advance satisfying $\sin\mu = 0$. The parallel-to-point imaging mode is achieved with the phase-advance satisfying $\cos\mu = 0$.

The rotatorlike matrix format given by Eq. (8) in Sec. III B is generally obtained by matching identical output betas, and identical output alphas in the two transverse planes, plus the horizontal phase advance, μ_x, and the vertical phase advance, μ_z, satisfying:

$$\cos\mu_x = -\cos\mu_z, \quad \text{and} \quad \sin\mu_x = -\sin\mu_z, \quad (18)$$

which is equivalent to a single constraint:

$$|\mu_x - \mu_z| = (2n+1)\pi, \text{ where } n \text{ is an integer number.} \quad (19)$$

Usually, $n = 0$ for short transfer lines like a gantry or a rotator.

This matching strategy was used in our previous works [34,35]. It is going to be applied also in this work using the WinAGILE (Windows Alternating Gradient Lattice Design) built-in matching routines [36].

C. Simulation tools

The rotatorlike gantry optics presented in this paper is based primarily on analytical calculations. Its application to the MedAustron gantry required matching the analytically formulated ion-optical constraints for a concrete configuration of the MedAustron gantry magnets. This configuration was fixed and could not be changed nor optimized. Merely the excitations of the seven (identical) gantry quadrupoles could be used as matching variables, keeping in mind the limit of the quadrupoles' power converters. This limit was $\lfloor kL \rfloor \leq 2$ m^{-1}, where k is the normalized quadrupole field-gradient, and L is the effective length of a quadrupole ($L = 30$ cm). The matching has been performed with the aid of the WinAGILE code [36]. This code has also been used to perform beam envelope calculations, scattering simulations, and to produce numerical data for graphical outputs presented in this paper.

WinAGILE is a beam-transport code based on the first-order 6×6 transfer-matrix formalism and Twiss formalism. It provides an immediate graphical output for all calculated quantities, like lattice functions, beam envelopes, single-particle trajectories, emittance diagrams and beam profiles in the phase space, beam-spots and beam profiles in the real space, 2D and 3D beamline geometries, and many others. It is equipped with powerful statistical routines to generate and analyze different beam distributions as well as effective and easy-to-control matching routines. It can also simulate beam scattering in several modes: (i) Twiss parameters, (ii) beam envelopes, and (iii) tracking distributions. The beam transport in the tracking distributions mode is presented in an animated way either in the phase space or in the real space. The obtained numerical and graphical results can be exported to different formats for further analysis and processing. We have used WinAGILE to design and explore numerous gantry versions. The designs of the most promising candidates have later been verified and refined with the aid of MAD-X/PTC (beam optics, particle tracking) [37] and FLUKA (scattering) [38] simulations in the framework of the MedAustron gantry beamline commissioning [21].

D. Initial gantry optics

The initial gantry optics was derived from the original PSI optics that was very close to the point-to-point imaging with magnification $M = 1$, horizontal phase advance $\mu_x = 3\pi$, and vertical phase advance $\mu_z = 2\pi$ [31,32]. The original PSI transfer matrix differs slightly from these exact values [31]. After some minor rematching, we arrived at the initial optics characterized by the transfer matrix, $\mathbf{R}_{\mathbf{GAN\_initial}}$:

$$\mathbf{R}_{\mathbf{GAN\_initial}} = \begin{pmatrix} -1.000 & 0 & 0 & 0 \\ -0.914 & -1.000 & 0 & 0 \\ 0 & 0 & 1.000 & 0 \\ 0 & 0 & 0 & 1.000 \end{pmatrix}. \quad (20)$$

The numbers in the transfer matrix are given in the SI units and rounded to three decimal digits. This format is going to be used through the whole paper. The phase advances correspond to the point-to-point imaging in both gantry

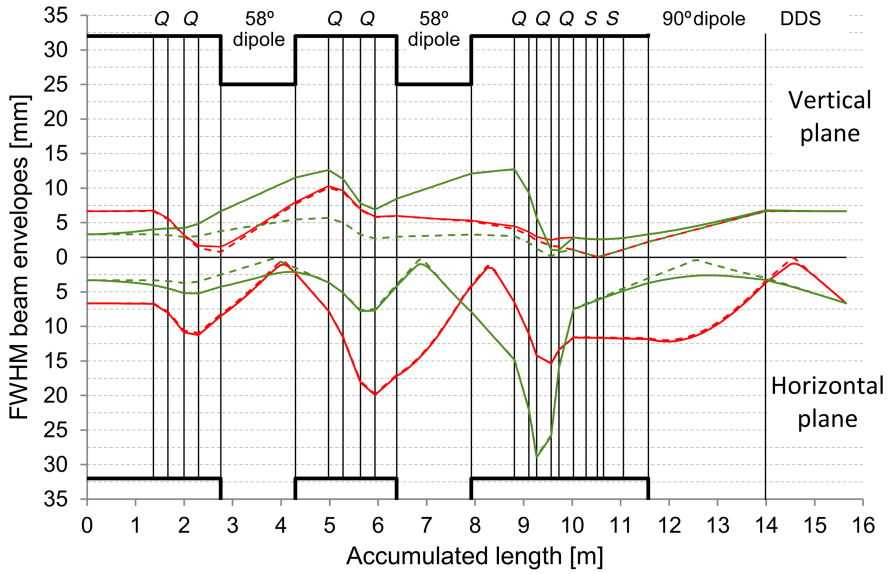

FIG. 2. Optical FWHM beam envelopes in the gantry for the initial gantry optics. Red envelopes: gantry magnification $M = 1$. Green envelopes: gantry magnification $M = 2$. Solid lines: full ellipse. Dashed lines: bar. Vertical lines: position of the main gantry elements (Q, quadrupoles and S, scanning magnets). DDS: dose delivery system. Thick black lines: vacuum chamber aperture. Upper half of the plot: the vertical gantry plane and lower half of the plot: the horizontal gantry plane.

transverse planes and satisfy the constraint (19) for the rotatorlike matrix format. However, it is not the rotatorlike optics yet, because $g_{43} \neq -g_{21}$. This is because the output alphas at the isocenter are different in the two gantry transverse planes. While there is a beam waist in the vertical plane ($\alpha_v = 0$), a divergent beam ($\alpha_h < 0$) occurs in the horizontal plane (the beam envelopes are going to be shown below in Sec. V A, Fig. 2). The seven gantry quadrupoles are involved in matching the transfer matrix terms as follows: one for the horizontal beta function, one for the vertical beta function, one for the horizontal phase advance, one for the vertical phase advance, two for the dispersion function and its derivatives, and one for the vertical alpha. There is no free quadrupole left for matching the horizontal alpha.

This so-called initial gantry optics was the point the evolution of the rotatorlike gantry optics started from.

V. EVOLUTION OF THE ROTATORLIKE GANTRY OPTICS

A. Identification and formulation of the problem

The initial optics is close to the original PSI optics that was originally designed for beams served by a cyclotron [31,32]. Application of the initial optics to the slowly extracted asymmetric beams from the MedAustron medical synchrotron revealed some serious beam transport problems. Figure 2 shows the optical (i.e., not scattered) FWHM beam envelopes in the gantry. Two different gantry magnifications have been investigated.

The first case—the red envelopes—corresponds to the gantry magnification $M = 1$. The input Twiss parameters (in both planes) are $\beta = 8$ m, $\alpha = 0$, and $\varepsilon = 1$ πmm mrad and $\beta = 800$ m, $\alpha = 0$, and $\varepsilon = 0.01$ πmm mrad for the full ellipse and for the bar, respectively. These input Twiss parameters have been chosen as an example to produce a round beam spot of about 6.7 mm FWHM at the gantry isocenter, which is within the medical specifications [21]. In addition, this choice makes it possible to produce the same output beam at the gantry isocenter with convenient values of input $\beta = 8$ m and $M = 1$, and $\beta = 2$ m and $M = 2$, since the point-to-point optics provides $\beta_{\text{out}} = M^2\beta_{\text{in}}$. Comparing the situations with two different gantry magnifications is going to be useful to demonstrate the problem with the initial gantry optics. It should be noted that calculating (scaling) the Twiss parameters for the full ellipse and for the bar is based on Eqs. (3), (4), and (11) for a chosen emittance ratio $\frac{\varepsilon_{\text{bar}}}{\varepsilon_{\text{full ellipse}}} = 1\%$.

Since the input beam satisfies the sigma-matching constraint given by Eq. (11), and the gantry optics satisfies the corresponding constraints given by Eq. (12), the beam spot is independent from the gantry rotation angle. Unfortunately, this can be true for the gantry isocenter only since all matched ion-optical constraints are applied exactly at the gantry isocenter. There are no free quadrupoles left to control the beam at some other significant gantry elements, namely at the DDS monitors located downstream of the last gantry dipole. At the DDS monitors, this optics entirely fails. In the horizontal plane, the beam is: (i) too small to be measured reliably, (ii) not round, (iii) very much different from the beam at the isocenter, and (iv) going to scatter differently from the beam scattering in the vertical plane. It can be seen that these problems do not exist in the vertical plane, where—thanks to the beam waist

at the gantry isocenter—the beam at the DDS monitors is practically identical to the beam at the isocenter. This stimulates looking for the optics forming the waist at the isocenter in both gantry planes.

One can try to improve the situation by a different combination of the gantry magnification and the input Twiss parameters, as anticipated above. For example, the green envelopes correspond to the gantry magnification $M = 2$, and the input Twiss parameters (in both planes) $\beta = 2$ m, $\alpha = 0$, and $\varepsilon = 1\pi$ mm mrad and $\beta = 200$ m, $\alpha = 0$, $\varepsilon = 0.01$ πmm mrad for the full ellipse and for the bar, respectively. This produces the same output beam spot at the gantry isocenter as in the previous case (the red envelopes). Although the situation improves slightly at the DDS monitors, the horizontal beam envelope gets too close to the vacuum chamber inside the gantry, and the excitations of the last quadrupole triplet go beyond the power converter limit. It is still theoretically impossible to form the waist at the isocenter in both gantry planes simultaneously. More strictly speaking, it is impossible to achieve the waist-to-waist transformation in both planes simultaneously.

B. Rotatorlike gantry optics

The problem must be solved differently and can be solved in two steps.

In the first step, it is necessary to get identical beam envelopes in the gantry nozzle in the two gantry transverse planes. This mathematically means expanding the sigma-matching principle also to the covariance terms of the beam sigma matrix at the gantry isocenter, Σ_{12} and Σ_{34}. The procedure is the same as in Refs. [22,23] for the variance terms Σ_{11} and Σ_{33}. Performing the sigma-matrix transformation (7) yields

$$\Sigma_{12} = g_{11}g_{21}(\sigma_{11}C^2 + \sigma_{33}S^2) + (g_{21}g_{12} + g_{22}g_{11}) \times (\sigma_{12}C^2 + \sigma_{34}S^2) + g_{22}g_{12}(\sigma_{22}C^2 + \sigma_{44}S^2), \quad (21)$$

$$\Sigma_{34} = g_{33}g_{43}(\sigma_{33}C^2 + \sigma_{11}S^2) + (g_{34}g_{43} + g_{33}g_{44}) \times (\sigma_{34}C^2 + \sigma_{12}S^2) + g_{34}g_{44}(\sigma_{44}C^2 + \sigma_{22}S^2), \quad (22)$$

where $C = \cos\varphi$ and $S = \sin\varphi$, with φ being the gantry rotation angle. In the point-to-point sigma-matching mode, the constraints $g_{12} = g_{34} = 0$ and $\sigma_{11} = \sigma_{33}$ apply, which simplifies Eqs. (21) and (22) to:

$$\Sigma_{12} = g_{11}g_{21}\sigma_{11\equiv 33} + g_{22}g_{11}(\sigma_{12}C^2 + \sigma_{34}S^2), \quad (23)$$

$$\Sigma_{34} = g_{33}g_{43}\sigma_{11\equiv 33} + g_{33}g_{44}(\sigma_{34}C^2 + \sigma_{12}S^2). \quad (24)$$

Eliminating the angular dependence is possible with $\sigma_{12} = \sigma_{34}$ since $C^2 + S^2 = 1$:

$$\Sigma_{12} = g_{11}g_{21}\sigma_{11\equiv 33} + g_{22}g_{11}\sigma_{12\equiv 34}, \quad (25)$$

$$\Sigma_{34} = g_{33}g_{43}\sigma_{11\equiv 33} + g_{33}g_{44}\sigma_{12\equiv 34}. \quad (26)$$

This shows that the sigma-matching principle can be expanded also to the covariance terms of the beam sigma matrix at the gantry isocenter. The beam served at the gantry entrance with identical horizontal and vertical beam sizes ($\sigma_{11} = \sigma_{33}$) and covariances ($\sigma_{12} = \sigma_{34}$) will have angularly independent covariances at the gantry isocenter in addition to the angularly independent beam size. Asking for identical covariances means

$$\Sigma_{12} = \Sigma_{34} \Rightarrow g_{11}g_{21}\sigma_{11\equiv 33} + g_{22}g_{11}\sigma_{12\equiv 34} = g_{33}g_{43}\sigma_{11\equiv 33} + g_{33}g_{44}\sigma_{12\equiv 34}. \quad (27)$$

Because the determinant of the gantry transfer matrix in both transverse planes must be 1, the following relations hold for the point-to-point transfer matrix:

$$g_{11}g_{22} = 1 \quad \text{and} \quad g_{33}g_{44} = 1. \quad (28)$$

Equation (27) then simplifies to:

$$\Sigma_{12} = \Sigma_{34} \Rightarrow g_{11}g_{21} = g_{33}g_{43}. \quad (29)$$

It has to be remembered that sigma matching requires also $|g_{11}| = |g_{33}|$ [Sec. III C, Eq. (12)], which is implemented in our design as $g_{11} = -g_{33}$. Equation (29) is then satisfied with $g_{21} = -g_{43}$, which completes the rotatorlike format of the whole gantry transfer matrix. In other words, it has been shown that the rotatorlike optics leads to identical and angularly independent covariance terms of the beam sigma matrix at the gantry isocenter. Once they are identical and angularly independent, they can be controlled by a proper adjustment of the covariance terms of the incoming beam sigma matrix at the gantry entrance, which is the second step of the solution presented in this paper. This—a (nonwaist)-to-waist transformation—is going to be shown in the next section.

The parallel-to-point sigma-matching mode can be treated in the same manner and leads to the same result. Therefore, only the main calculation steps are going to be resumed. With the parallel-to-point sigma-matching constraints (14) and (15), Eqs. (21) and (22) simplify to:

$$\Sigma_{12} = g_{21}g_{12}(\sigma_{12}C^2 + \sigma_{34}S^2) + g_{22}g_{12}\sigma_{22\equiv 44}, \quad (30)$$

$$\Sigma_{34} = g_{34}g_{43}(\sigma_{34}C^2 + \sigma_{12}S^2) + g_{34}g_{44}\sigma_{22\equiv 44}. \quad (31)$$

Taking into account $g_{21}g_{12} = g_{34}g_{43} = -1$, $g_{12} = -g_{34}$ (this must be foreseen in the parallel-to-point design), and

setting $\sigma_{12} = \sigma_{34} = \sigma_{12\equiv 34}$ finally leads to $g_{22} = -g_{44}$ to satisfy $\Sigma_{12} = \Sigma_{34}$.

C. Results

In the point-to-point sigma-matching mode, we have generated rotatorlike gantries with magnification from 0.8 up to 2.5 in 0.1 steps. The seven gantry quadrupoles are involved in matching the transfer matrix terms as follows: one for the horizontal beta function, one for the vertical beta function, one for the horizontal phase advance, one for the vertical phase advance, two for the dispersion function and its derivatives, and one for equal alphas in the two transverse planes. One can only ask for equal alphas without having a possibility to set their value. In the first step, one has to tolerate the matching result. In the second step, one can adjust the input Twiss parameters at the gantry entrance to obtain desirable Twiss parameters (including alphas) at the gantry isocenter.

Among all point-to-point rotatorlike gantries under study, the gantry with magnification $M = 1$ provided the smallest beam envelopes inside the gantry. After matching the equal alphas constraint, its transfer matrix, $\mathbf{R}_{\mathbf{GAN\_RLG1.0}}$, becomes

$$\mathbf{R}_{\mathbf{GAN\_RLG1.0}} = \begin{pmatrix} -1.000 & 0 & 0 & 0 \\ -0.870 & -1.000 & 0 & 0 \\ 0 & 0 & 1.000 & 0 \\ 0 & 0 & 0.870 & 1.000 \end{pmatrix}, \tag{32}$$

which is the rotatorlike matrix format. The corresponding optical FWHM beam envelopes are shown in Fig. 3.

The green envelopes correspond to the beam waist at the gantry entrance. The input Twiss parameters (in both planes) are $\beta = 6.492$ m, $\alpha = 0$, and $\varepsilon = 1$ πmm mrad and $\beta = 649.224$ m, $\alpha = 0$, $\varepsilon = 0.01$ πmm mrad for the full ellipse and for the bar, respectively. The bar is flat in the phase space. This produces a round beam spot of 6 mm FWHM at the gantry isocenter. Since the gantry optics satisfies the rotatorlike constraints, not only the beam spot but also the $\langle xx' \rangle$ and $\langle zz' \rangle$ covariances are independent from the gantry rotation angle (and the same in the two gantry transverse planes) at the gantry isocenter. This makes it possible to control them by adjustment of the input Twiss parameters as shown by the red envelopes. They were calculated to reach desired beam parameters at the gantry isocenter, namely again the spot of 6 mm FWHM, but this time with the beam waist in both transverse planes. The beam waist is a natural (but not necessary) choice to get practically identical beam parameters at the gantry isocenter and the DDS monitors. This can be a subject of further optimization and the users may ask—besides the beam waist—for convergent or divergent beams, too, according to their specific needs.

The input beam parameters at the gantry entrance for the red envelopes can be calculated either by inverting the transformation (7), which is the most general approach, or from the following relations that take already into account the specific point-to-point imaging conditions. The beam size at the gantry entrance is determined by the required beam size at the gantry isocenter, $\sqrt{\Sigma_{11\equiv 33}}$, that is a medical specification, and the gantry magnification, M:

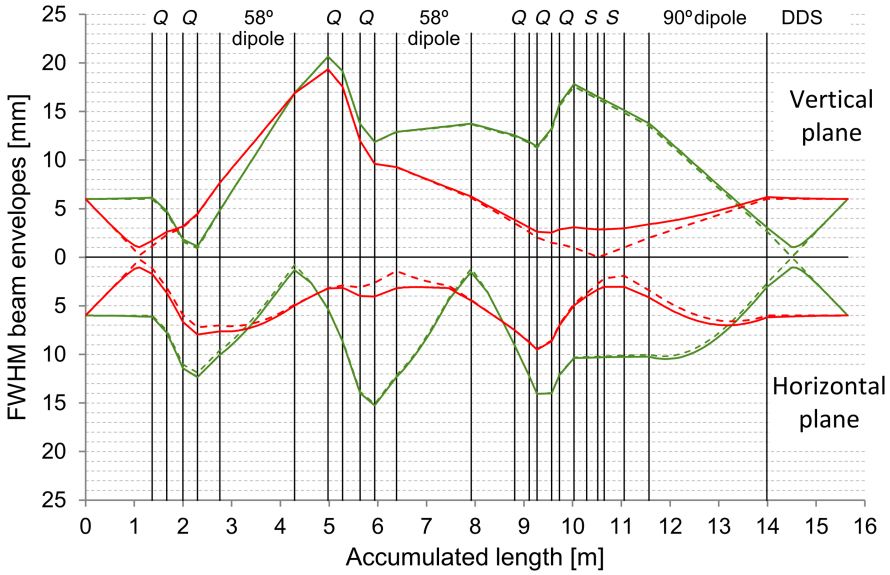

FIG. 3. Optical (without scattering) FWHM beam envelopes in the gantry for the rotatorlike gantry optics. Red envelopes: beam waist at the gantry isocenter. Green envelopes: beam waist at the gantry entrance. Solid lines: full ellipse. Dashed lines: bar. Vertical lines: position of the main gantry elements (Q, quadrupoles and S, scanning magnets). DDS: dose delivery system. Upper half of the plot: the vertical gantry plane and lower half of the plot: the horizontal gantry plane.

$$\sqrt{\Sigma_{11\equiv 33}} = M\sqrt{\sigma_{11\equiv 33}} \Rightarrow \sigma_{11\equiv 33} = \frac{\Sigma_{11\equiv 33}}{M^2} = \frac{\Sigma_{11\equiv 33}}{g_{11}^2} \quad (33)$$

since the magnification, $M = |g_{11}|$ according to its definition (12) in Sec. III C. Plugging Eq. (33) into Eq. (25) yields

$$\begin{aligned}\sigma_{12\equiv 34} &= \Sigma_{12\equiv 34} - g_{11}g_{21}\sigma_{11\equiv 33} \\ &= \Sigma_{12\equiv 34} - g_{11}g_{21}\frac{\Sigma_{11\equiv 33}}{g_{11}^2} = \Sigma_{12\equiv 34} - \frac{g_{21}}{g_{11}}\Sigma_{11\equiv 33}.\end{aligned} \quad (34)$$

For the red envelopes presented in Fig. 3, the output beam spot was set to 6 mm FWHM, and $\Sigma_{12\equiv 34} = 0$, which is equivalent to the beam waist at the gantry isocenter. The corresponding input Twiss parameters (in both planes) are $\beta = 6.492$ m, $\alpha = 5.646$, and $\varepsilon = 1$ πmm mrad and $\beta = 649.224$ m, $\alpha = 564.582$, and $\varepsilon = 0.01$ πmm mrad for the full ellipse and for the bar, respectively.

No general statement can be made concerning feasibility of the beam parameters at the gantry entrance. This must be checked individually for each incoming beamline the gantry is connected to.

In the parallel-to-point sigma-matching mode, we have generated rotatorlike gantries with magnification from 1.4 up to 4.1 m in 0.1 m steps. The seven gantry quadrupoles are involved in matching the transfer matrix terms as follows: one for the horizontal beta function, one for the vertical beta function, one for the horizontal phase advance ($\mu_x = 2.5\pi$ in this case), one for the vertical phase advance ($\mu_z = 1.5\pi$ in this case), two for the dispersion function and its derivatives, and one for equal alphas in the two transverse planes. Favorable beam envelopes inside the gantry occurred with magnification from about 2 to 3 m. An example is presented in Fig. 4 for the parallel-to-point rotatorlike gantry with magnification 3 m. The corresponding transfer matrix, $\mathbf{R}_{\mathbf{GAN\_RLG3.0}}$, reads

$$\mathbf{R}_{\mathbf{GAN\_RLG3.0}} = \begin{pmatrix} 0.000 & 3.000 & 0 & 0 \\ -0.333 & 0.247 & 0 & 0 \\ 0 & 0 & 0 & -3.000 \\ 0 & 0 & 0.333 & -0.247 \end{pmatrix} \quad (35)$$

and the lattice functions are depicted in Fig. 5 for the input Twiss parameters $\beta = 1$ m and $\alpha = 0$ in both gantry transverse planes.

There are again two beams shown in Fig. 4. They both are designed to produce 6 mm FWHM beam spot at the gantry isocenter. The first beam—the green envelopes—is served with the beam waist at the gantry entrance. The input Twiss parameters (in both planes) are $\beta = 1.386$ m, $\alpha = 0$, and $\varepsilon = 1$ πmm mrad and $\beta = 0.014$ m, $\alpha = 0$, and $\varepsilon = 0.01$ πmm mrad for the full ellipse and for the bar, respectively. The bar is upright in the phase space. The second beam—the red envelopes—is designed to produce the beam waist at the gantry isocenter. The corresponding input Twiss parameters (in both planes) are $\beta = 1.784$ m, $\alpha = -0.536$, and $\varepsilon = 1$ πmm mrad and $\beta = 39.776$ m, $\alpha = -53.556$, and $\varepsilon = 0.01$ πmm mrad for the full ellipse and for the bar, respectively. Calculating (scaling) the Twiss

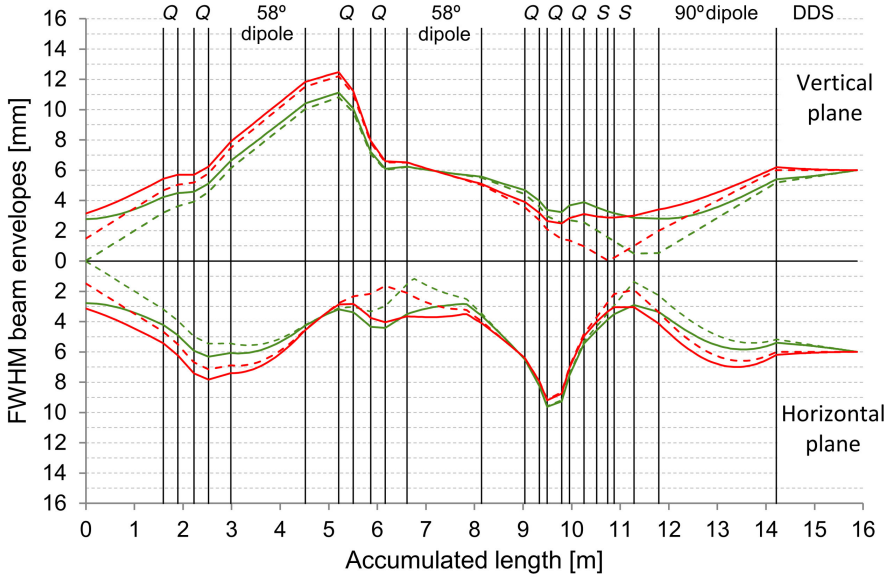

FIG. 4. Optical (without scattering) FWHM beam envelopes in the parallel-to-point gantry with magnification 3 m for the rotatorlike gantry optics. Red envelopes: beam waist at the gantry isocenter. Green envelopes: beam waist at the gantry entrance. Solid lines: full ellipse. Dashed lines: bar. Vertical lines: position of the main gantry elements (Q, quadrupoles and S, scanning magnets). DDS: dose delivery system. Upper half of the plot: the vertical gantry plane and lower half of the plot: the horizontal gantry plane.

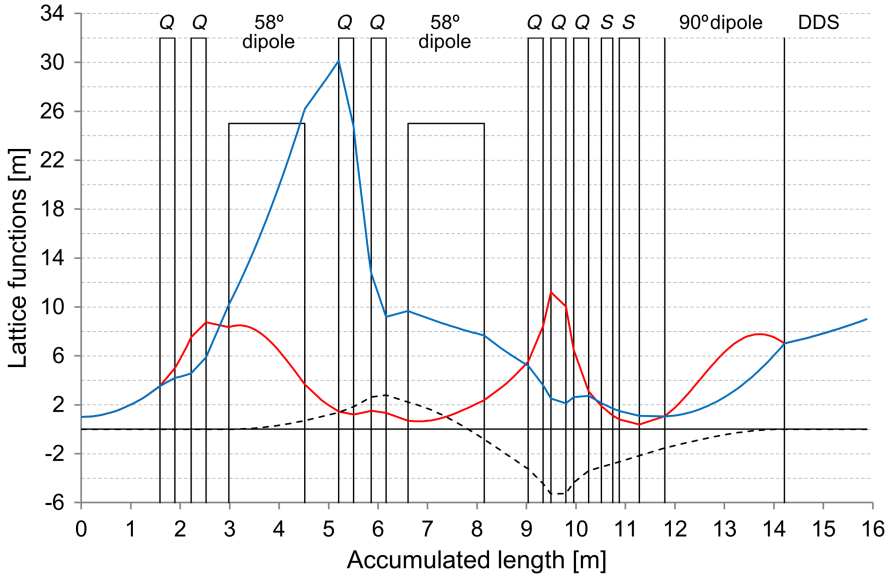

FIG. 5. Lattice functions in the parallel-to-point gantry with magnification 3 m for the rotatorlike gantry optics. Red solid line: horizontal beta function, blue solid line: vertical beta function, black dashed line: horizontal dispersion function, and vertical lines: position of the main gantry elements (Q, quadrupoles and S, scanning magnets). DDS: dose delivery system.

parameters for the full ellipse and for the bar is based on Eqs. (3), (4), and (14) for a chosen emittance ratio $\frac{\varepsilon_{\text{bar}}}{\varepsilon_{\text{full ellipse}}} = 1\%$.

VI. DISCUSSION

A. Point-to-point versus parallel-to-point

According to our study, the MedAustron proton gantry should be best run in the parallel-to-point rotatorlike mode with magnification of 3 m. This setting has been also recommended and used as the starting point for the MedAustron gantry beamline commissioning [21]. Compared to the point-to-point rotatorlike gantry, it provides smaller beam envelopes inside the gantry (compare Figs. 3 and 4 and notice the different vertical scales in those two figures). The required beam parameters at the gantry entrance are quite feasible and can be delivered by the incoming high-energy beam transfer (HEBT) line as verified during the gantry beamline commissioning. The output beam parameters satisfy the medical specifications at the gantry isocenter as well as at the DDS monitors. In addition to this, the beam size (without scattering) at the DDS monitors is almost identical to the one at the gantry isocenter. This is an advantage of the new, rotatorlike ion-optical concept with respect to the initial gantry optics.

Another useful advantage of the parallel-to-point imaging optics is its higher optical flexibility compared to the point-to-point imaging optics. More specifically, changing the drift-space length at the gantry entrance keeps the parallel-to-point imaging optics, since an input parallel ray stays parallel for any input drift-space length. This benefit has been exploited during the gantry beamline commissioning. Careful comparison of Figs. 3 and 4 reveals that the parallel-to-point gantry is slightly (by 22.5 cm) longer than the point-to-point one. This is due to an extra 22.5 cm long drift space at the gantry entrance coming from redefining of some of the HEBT modules. More specifically, this drift space was originally considered to belong to the deflection module upstream of the gantry entrance. With a new definition of the HEBT modules, it is now considered to belong to the gantry (see Ref. [21] for further details).

B. Beam divergence

From the point of view of patient-irradiation conditions, the most important beam property at the gantry isocenter is the beam spot that must be round. The shape of the beam spot directly influences the dose distribution in the patient body. Other properties are less critical, but they are strongly related to simplicity and reliability of the gantry-beamline operation. This is especially true for the angular independence of the beam spot at the gantry exit, which reduces dramatically the amount of gantry settings that need to be stored and commissioned. Finally, the equal and rotationally independent position-to-angular correlations in both gantry planes make it possible to optimize the shape of the beam envelopes downstream of the last gantry dipole, which is important for the DDS monitoring system. The least critical beam parameter from the ion optics point of view is its divergence, because—due to the scattering in the gantry nozzle—it is not going to be preserved. This is going to be investigated in Sec. VI C. In this section, the beam

divergence as determined by the ion optics is still going to be discussed, since it belongs to the general theoretical background of the rotatorlike optics.

The sigma-matching rotatorlike optics guarantees at the gantry isocenter:

$$\Sigma_{11\equiv 33} \neq f(\varphi) \quad \text{and} \quad \Sigma_{12\equiv 34} \neq f(\varphi). \tag{36}$$

The only parameter that remains a function of the gantry rotation angle, φ, is the beam divergence related to the Σ_{22} and Σ_{44} beam sigma-matrix terms at the gantry isocenter. Performing transformation (7) yields in general:

$$\Sigma_{22} = g_{21}^2(\sigma_{11}C^2 + \sigma_{33}S^2) + 2g_{21}g_{22}(\sigma_{12}C^2 + \sigma_{34}S^2) + g_{22}^2(\sigma_{22}C^2 + \sigma_{44}S^2), \tag{37}$$

$$\Sigma_{44} = g_{43}^2(\sigma_{33}C^2 + \sigma_{11}S^2) + 2g_{43}g_{44}(\sigma_{34}C^2 + \sigma_{12}S^2) + g_{44}^2(\sigma_{44}C^2 + \sigma_{22}S^2), \tag{38}$$

where $C = \cos\varphi$ and $S = \sin\varphi$, φ being the gantry rotation angle. In the point-to-point sigma-matching rotatorlike mode, they simplify to:

$$\Sigma_{22} = g_{21}^2\sigma_{11\equiv 33} + 2g_{21}g_{22}\sigma_{12\equiv 34} + g_{22}^2(\sigma_{22}C^2 + \sigma_{44}S^2), \tag{39}$$

$$\Sigma_{44} = g_{21}^2\sigma_{11\equiv 33} + 2g_{21}g_{22}\sigma_{12\equiv 34} + g_{22}^2(\sigma_{44}C^2 + \sigma_{22}S^2). \tag{40}$$

Notice that the vertical transfer-matrix terms in Eq. (40) have been replaced by the horizontal ones thanks to the rotatorlike matrix format. Similarly, in the parallel-to-point sigma-matching rotatorlike mode:

$$\Sigma_{22} = g_{21}^2(\sigma_{11}C^2 + \sigma_{33}S^2) + 2g_{21}g_{22}\sigma_{12\equiv 34} + g_{22}^2\sigma_{22\equiv 44}, \tag{41}$$

$$\Sigma_{44} = g_{21}^2(\sigma_{33}C^2 + \sigma_{11}S^2) + 2g_{21}g_{22}\sigma_{34\equiv 12} + g_{22}^2\sigma_{22\equiv 44}. \tag{42}$$

As an example, Fig. 6 shows the optical (i.e., without scattering) 1 rms beam divergence as a function of the gantry rotation angle for the green envelopes in Fig. 4. The input entries are $\sigma_{11} = 1.386$ mm^2, $\sigma_{12\equiv 34} = 0$, $\sigma_{22\equiv 44} = 0.721$ mrad^2, $\sigma_{33} = 1.386 \times 10^{-4}$ mm^2, and the transfer-matrix terms can be found in Eq. (35) that corresponds to the parallel-to-point rotatorlike gantry optics with magnification 3 m.

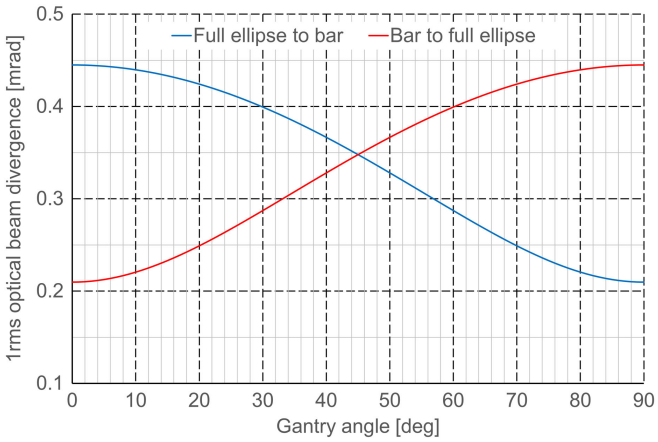

FIG. 6. Optical (without scattering) 1 rms beam divergence at the gantry isocenter as a function of the gantry rotation angle. The input beam parameters correspond to the green envelopes in Fig. 4. The gantry is tuned for parallel-to-point rotatorlike optics with magnification 3 m.

The transition from a bar to a full ellipse can be better observed with the aid of emittance diagrams. Let us use again the green envelopes in Fig. 4 and the corresponding analytical curves in Fig. 6 as an example. The Twiss parameters (in both planes) at the fixed beamline exit are $\beta = 1.386$ m, $\alpha = 0$, $\varepsilon = 1$ πmm mrad, and $\beta = 0.014$ m, $\alpha = 0$, $\varepsilon = 0.01$ πmm mrad for the full ellipse and for the bar, respectively. The bar is upright in the phase space. Figure 7 presents the corresponding 2D-emittance diagrams at the fixed beamline exit [plot 7(a)], and at the gantry isocenter at the gantry rotation angles 0°, 15°, and 40° in plot 7(b), plot 7(c), and plot 7(d), respectively. Simply speaking, with gantry rotation from $\varphi = 0°$ to $\varphi = 90°$, the divergence and emittance of the bar increase up to the divergence and emittance of the full ellipse. At the same time, the divergence and emittance of the full ellipse decrease down to the divergence and emittance of the bar. The other two attributes of the emittance diagrams, namely the beam size and the position-to-angle covariance, remain constant because—according to the theoretical description—they are independent from the gantry rotation angle. In addition, they are identical in the horizontal and vertical planes at the gantry isocenter. At the gantry rotation angle 45°, both emittance patterns would be identical since the bar is on its "half-way" to the full ellipse and—at the same time—the full ellipse is on its half-way to the bar (see also Fig. 6 and Sec. VI E). Therefore, they must meet at the gantry rotation angle 45°. At the gantry rotation angle 90°, the emittance patterns would be entirely exchanged. Two emittance diagrams in one of the gantry transverse planes are always merged into a single plot to facilitate direct visual comparison. Each plot represents two beams in the

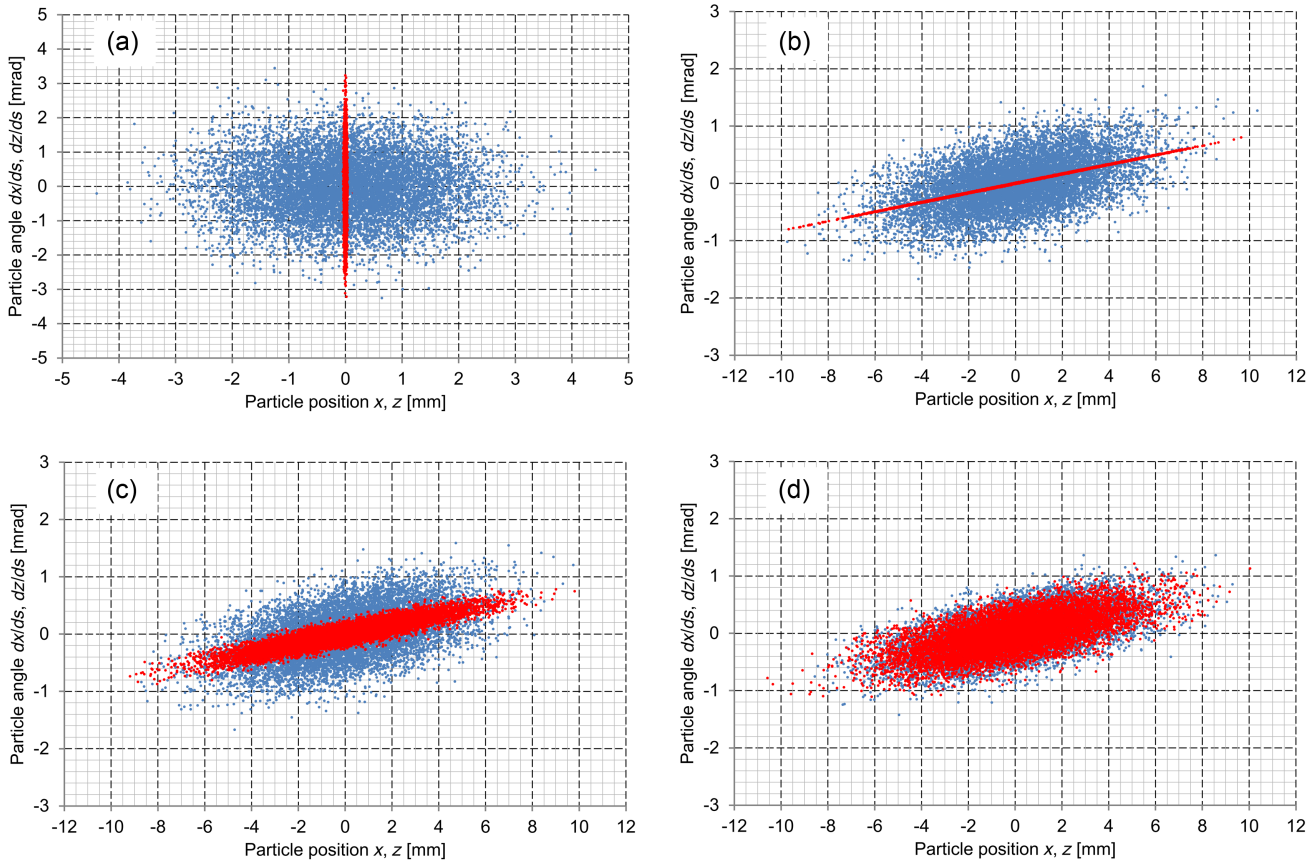

FIG. 7. Emittance diagrams of the input full-ellipse (blue) and the input bar (red) as a function of the gantry rotation angle without scattering. (a) Fixed beamline exit (5 rms cutoff, $\sigma_{22} = \sigma_{44}$, $\sigma_{12} = \sigma_{34} = 0$), (b) gantry isocenter, gantry rotation angle 0°, (c) gantry isocenter, gantry rotation angle 15°, and (d) gantry isocenter, gantry rotation angle 40°.

local gantry coordinate system corresponding to the bar and the full ellipse at the fixed beamline exit, simultaneously. It should be noted that the beam at the gantry isocenter is uncorrelated only at the gantry rotation angles 0° and ±90°. At all other gantry angles including the presented cases of 15° and 40°, there will be a correlation between the horizontal and vertical planes. Nevertheless, this correlation does not concern the beam spot in the real space [see Eq. (13) in Sec. III C]. The Σ_{13} correlation term at the gantry isocenter remains zero at all gantry rotation angles.

The section dealing with the beam divergence completes theoretical description and analysis of the sigma-matching rotatorlike working principle. In reality, the beam divergence as determined by ion optics is of less concern because it is going to be essentially altered by the beam scattering in the gantry nozzle. This is going to be discussed in the next section.

C. Beam scattering

Beam scattering in the gantry nozzle and in the air gap in front of the patient is a phenomenon that cannot be neglected in the final design and optimization of the gantry [39,40]. This is true for the design of the gantry optics as well as the gantry nozzle. In the case of the asymmetric beams, it is also very important to design the gantry in such a way that the scattered bar and the scattered full ellipse produce round and rotationally independent beam spot at the gantry isocenter. This medical requirement is usually expressed in terms of the beam full width at half maximum (FWHM). The gantry design must, therefore, take into account also possible differences in the rms-to-FWHM ratio between the bar and the full ellipse. Because the beam scattering depends on many circumstances including the orientation of the emittance diagram in the phase space, it is not sufficient to rely on a simplified expectation that the optically matched beams remain matched also after beam scattering. The rotatorlike gantry optics reduces dramatically the complexity of calculating the beam transport with scattering.

Let us assume a rotator followed (or preceded) by a drift space. When the drift space—for example—follows the rotator, the transfer matrix of the whole ion-optical system reads

$$\mathbf{R}_{\mathbf{ROT+DRIFT}} = \begin{pmatrix} 1 & L & 0 & 0 \\ 0 & 1 & 0 & 0 \\ 0 & 0 & 1 & L \\ 0 & 0 & 0 & 1 \end{pmatrix} \begin{pmatrix} r_{11} & r_{12} & 0 & 0 \\ r_{21} & r_{22} & 0 & 0 \\ 0 & 0 & -r_{11} & -r_{12} \\ 0 & 0 & -r_{21} & -r_{22} \end{pmatrix}, \tag{43}$$

where L is the drift-space length. Performing the matrix multiplication yields

$$\mathbf{R}_{\mathbf{ROT+DRIFT}} = \begin{pmatrix} r_{11}+Lr_{21} & r_{12}+Lr_{22} & 0 & 0 \\ r_{21} & r_{22} & 0 & 0 \\ 0 & 0 & -(r_{11}+Lr_{21}) & -(r_{12}+Lr_{22}) \\ 0 & 0 & -r_{21} & -r_{22} \end{pmatrix}, \tag{44}$$

which keeps the rotatorlike matrix format. It means that adding a drift space behind a rotator preserves the rotator properties of the whole system. The same is true for a drift space in front of a rotator. This property has a simple interpretation. If a rotator is followed (or preceded) by a drift, particle trajectories are going to be the same regardless of the drift being rotated or not because no forces are acting on the particles in the drift. That is why one can imagine that the drift is rotated together with the rotator even without mechanical rotation of the drift vacuum chamber. The rotated drift is—from the ion-optical point of view—equivalent to the drift that is a part of the rotator. In other words, it is not relevant whether the coordinate system rotations are considered at the beginning or at end of the drift. The overall transfer matrix of the whole structure consisting of the rotator and the additional drifts will be the same regardless of this choice. This can be proven by performing the matrix multiplication:

$$\begin{aligned} &\begin{pmatrix} 1 & L & 0 & 0 \\ 0 & 1 & 0 & 0 \\ 0 & 0 & 1 & L \\ 0 & 0 & 0 & 1 \end{pmatrix} \begin{pmatrix} C & 0 & S & 0 \\ 0 & C & 0 & S \\ -S & 0 & C & 0 \\ 0 & -S & 0 & C \end{pmatrix} \\ &= \begin{pmatrix} C & 0 & S & 0 \\ 0 & C & 0 & S \\ -S & 0 & C & 0 \\ 0 & -S & 0 & C \end{pmatrix} \begin{pmatrix} 1 & L & 0 & 0 \\ 0 & 1 & 0 & 0 \\ 0 & 0 & 1 & L \\ 0 & 0 & 0 & 1 \end{pmatrix} \end{aligned} \tag{45}$$

representing the transfer matrix of a drift space with length L that is preceded [left side of Eq. (45)] or followed [right side of Eq. (45)] by the coordinate system rotation, where $C = \cos\frac{\varphi}{2}$ and $S = \sin\frac{\varphi}{2}$. The transfer matrix of a drift with the coordinate system rotation is the same for the coordinate system rotation taking place at the beginning or at the end of the drift. Although this is true for any angle, we present it for the gantry rotation angle, φ.

Let us now apply this finding to the gantry optics. If the gantry transfer matrix (from the gantry entrance to the gantry isocenter) is a rotatorlike matrix, the transfer matrix from the gantry entrance to the vacuum window will also be a rotatorlike matrix, because the part of the gantry beamline from the vacuum window to the isocenter is a drift space. For example, the transfer matrix from the gantry entrance to the vacuum window for the gantry shown in Fig. 4, $\mathbf{R}_{\mathbf{GAN\_RLG3.0\_WINDOW}}$, reads

$$\mathbf{R}_{\mathbf{GAN\_RLG3.0\_WINDOW}} = \begin{pmatrix} 0.385 & 2.714 & 0 & 0 \\ -0.333 & 0.247 & 0 & 0 \\ 0 & 0 & -0.385 & -2.714 \\ 0 & 0 & 0.333 & -0.247 \end{pmatrix}. \tag{46}$$

Let us imagine a virtual rotation of the gantry local coordinate system at the vacuum window by the gantry rotation angle, φ. According to the rotator working principle, the beam emittance diagrams in this virtually rotated coordinate system must be the same for all gantry angles (all individual beam particles keep their coordinates at the vacuum window in the virtually rotated coordinate system). This practically means that the beam scattering starts from absolutely identical emittance pattern regardless of the gantry angle. It makes it possible to compensate easily for all scattering-related effects by proper adjustment of the incoming beam to obtain a perfectly round beam spot at the gantry isocenter. The adjustment of the incoming beam is going to be universally valid for all gantry angles.

Following the gantry rotation, the scattered beam spot at the gantry isocenter is going to rotate, too. This rotation cannot be avoided as it is the fundamental action of any rotator. Because the gantry has become a rotator in our design, it must rotate the beam spot by the gantry rotation angle φ (in the local gantry coordinate system) at any location downstream of the exit from the last gantry dipole. Nevertheless, supposing the scattered beam spot is round,

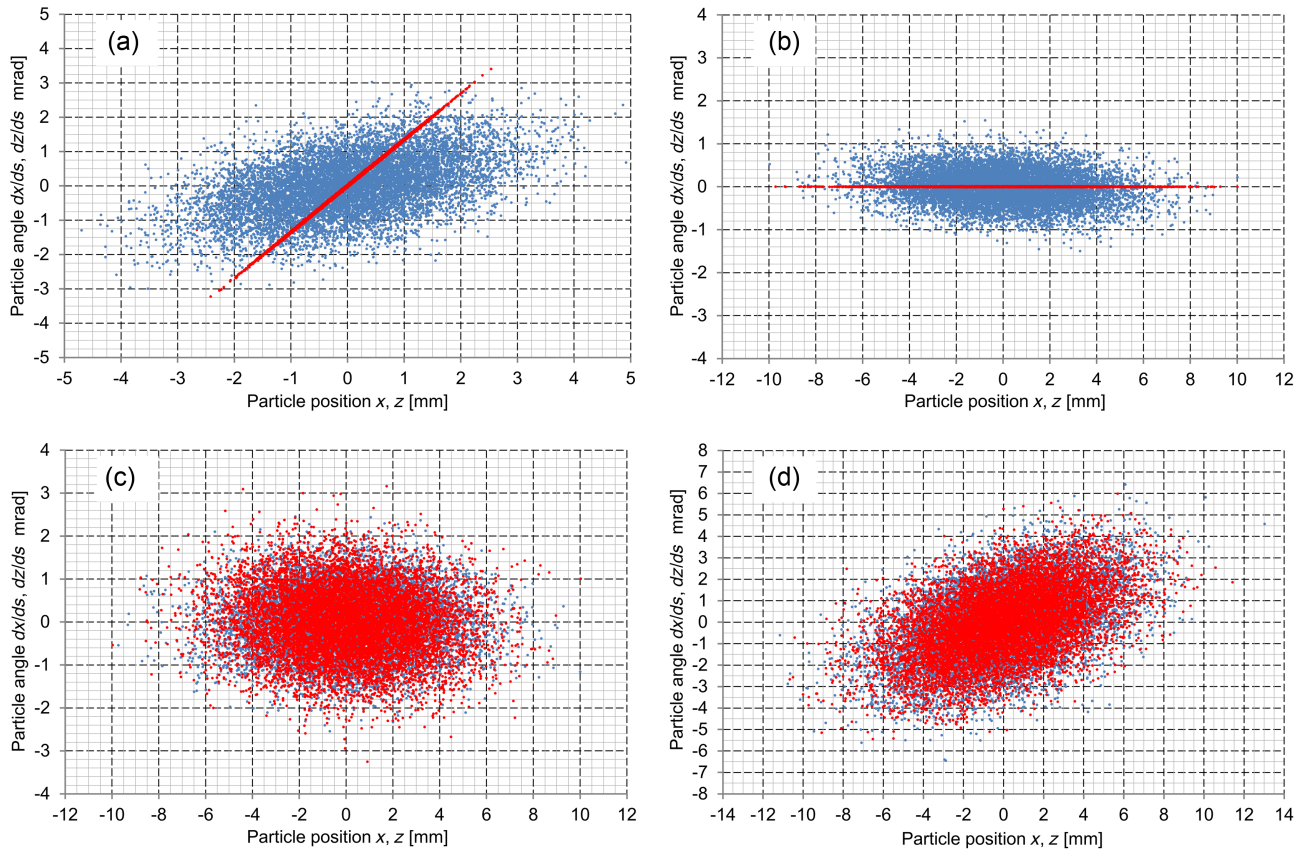

FIG. 8. Emittance diagrams of the full ellipse (blue) and the bar (red) including beam scattering in the gantry nozzle and in the air gap in front of the patient. (a) Gantry entrance ($\sigma_{22} = \sigma_{44}, \sigma_{12} = \sigma_{34} \neq 0$), (b) inner side of the vacuum window, (c) outer side of the vacuum window, and (d) gantry isocenter. Proton-beam energy is 252.7 MeV, and the particle distributions used for tracking are cut at 5 rms.

this rotation can be neglected. The beam roundness has been verified at the occasion of the MedAustron gantry beamline commissioning [21] and fitted very well with the medical specifications. It must be pointed out that this beam-spot rotation occurs only when no external rotator is used in the beamline the gantry is connected to.

Beam scattering can be effectively used to balance the emittances of the full ellipse and the bar, as described in Sec. III A. In our design, scattering in the gantry nozzle is used for this job. In combination with the rotatorlike optics, practically identical emittance diagrams of the full ellipse and the bar can be obtained at the gantry isocenter. Two parameters, $\Sigma_{11\equiv 33}$ and $\Sigma_{12\equiv 34}$, are matched by optical means thanks to the sigma-matching rotatorlike optics. The third parameter, the beam divergence, is then matched by scattering in the gantry nozzle and in the air gap in front of the patient. The situation is illustrated in Fig. 8 that shows the emittance patterns at four significant gantry places: (i) the exit of the incoming fixed beamline = the gantry entrance, (ii) the inner side of the vacuum window, (iii) the outer side of the vacuum window, and (iv) the gantry isocenter. Similar to Fig. 7, two emittance diagrams in one of the gantry transverse planes are always merged into a single plot to facilitate direct visual comparison. Each plot represents two beams in the local gantry coordinate system corresponding to the bar and the full ellipse at the fixed beamline exit, simultaneously.

The input parameters of the beam presented in Fig. 8 are identical to the input parameters of the beam presented in Fig. 4 by the red envelopes producing 6 mm FWHM beam waist at the gantry isocenter (without scattering). At the gantry entrance, $\beta = 1.784$ m, $\alpha = -0.536$, and $\varepsilon = 1\ \pi$mm mrad and $\beta = 39.776$ m, $\alpha = -53.556$, and $\varepsilon = 0.01\ \pi$mm mrad for the full ellipse and for the bar, respectively. They satisfy the constraints $\sigma_{22} = \sigma_{44}$ and $\sigma_{12} = \sigma_{34}$ as required for a parallel-to-point rotatorlike sigma-matching gantry. The proton-beam energy is 252.7 MeV. The emittance diagrams at the gantry entrance are depicted in the upper left plot [Fig. 8(a)]. The upper right plot [Fig. 8(b)] shows the emittance diagrams on the inner surface of the vacuum window, just before the scattering is going to start. The bar is flat in the phase space, which provides the maximum possible emittance blowup. This pattern appears at all gantry angles after rotating the vacuum window virtually by the gantry rotation angle. Thus the scattering always starts from the same initial emittance pattern. The lower left plot [Fig. 8(c)] shows the emittance diagrams on the outer (air) side of the

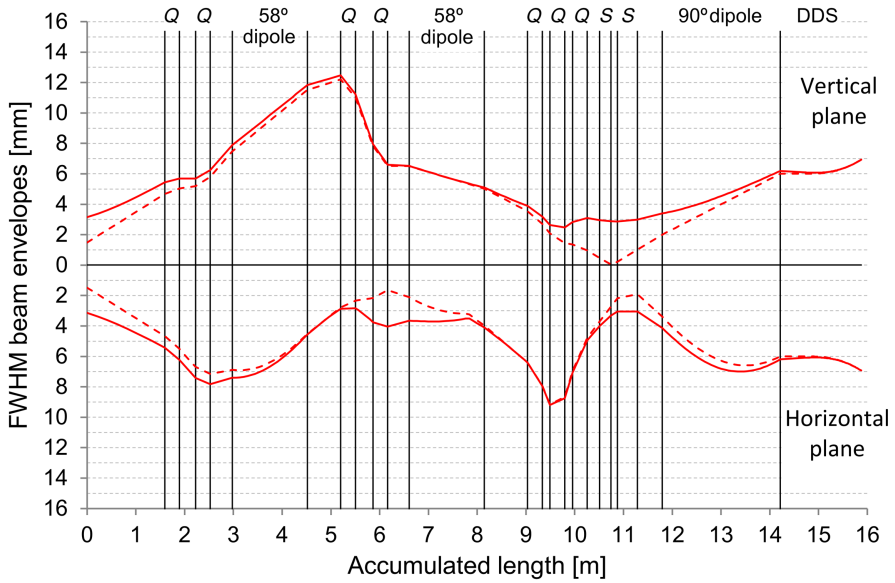

FIG. 9. FWHM beam envelopes in the parallel-to-point gantry with magnification 3 m for the rotatorlike gantry optics including beam scattering in the gantry nozzle for 252.7 MeV protons. Input beam parameters are identical to the input beam parameters in Fig. 4 as well as in Fig. 8. Solid lines: full ellipse, dashed lines: bar, and vertical lines: position of the main gantry elements (Q, quadrupoles and S, scanning magnets). DDS: dose delivery system. Upper half of the plot: the vertical gantry plane and lower half of the plot: the horizontal gantry plane.

vacuum window. It can be seen that already at this position, the emittance diagrams are almost equalized. This means that the vacuum window alone can play the role of a scattering foil used for the scattering-foil matching mentioned in Sec. III A. Scattering in the rest of the gantry nozzle further supports the emittance-balancing process as shown in the lower right plot [Fig. 8(d)] that completes the picture at the gantry isocenter.

The emittance diagrams at the gantry isocenter become practically identical [see the plot 8(d)]. They are very close to each other already at the outer (air) side of the vacuum window [see the plot 8(c)], which means that they are going to be close to each other also at the DDS monitors. In this way, rotation-independent beam transport can be achieved not just at the gantry isocenter (as it was the case in Fig. 2), but practically in the whole region downstream of the last dipole exit without the need for additional gantry quadrupoles. Since there is the least scattering at the top energy of 252.7 MeV, it will work also for lower proton-beam energies.

The real (scattered) beam has not exactly waist at the gantry isocenter as predicted by the ion optics [see the plot 8 (d)]. Rather than, it is slightly divergent, which is obviously caused by scattering in the gantry nozzle. Figure 9 shows the beam envelopes including beam scattering in the gantry nozzle for the 252.7 MeV proton beam as calculated by WinAGILE. The WinAGILE calculations have been later refined by FLUKA simulations using a more detailed model of the gantry nozzle. The FLUKA simulations are in good agreement with the beam-size measurements performed in the framework of the gantry beamline commissioning [21].

The beam scattering in the gantry nozzle can also be characterized by the evolution of the Twiss parameters, especially the beam emittance, in the gantry nozzle. Table I presents the Twiss parameters in the gantry nozzle for the 252.7 MeV proton beam as calculated by the WinAGILE code with the aid of a special lattice element called "scatterer."

The difference in beam emittance between the scattered bar and the scattered full ellipse at the gantry isocenter is less than 3%, which proves quantitatively our statement that the emittances are practically balanced. We have also calculated the final 1 rms beam divergence at the gantry isocenter given as $\sqrt{\gamma\varepsilon}$, where $\gamma = \frac{1+\alpha^2}{\beta}$. With the Twiss parameters from Table I, the beam divergence at the gantry isocenter is 1.872 mrad, and 1.830 mrad for the (original) full ellipse and (original) bar, respectively. The calculated beam size and the position-to-angle covariance for the full ellipse and for the bar are identical.

We have checked the scattering effect also for a 400 MeV/n carbon-ion beam. In order to facilitate a direct comparison, the same beam was assumed at the inner side of the vacuum window [see Fig. 8, plot 8(b)], just the particle species were changed from 252.7 MeV protons to 400 MeV/n carbon ions. Strictly speaking, the emittance pattern for carbon ions is not absolutely "the same" as for protons, but the difference is only within the statistical fluctuations. This is due to the fact that the routine used to generate the particle distributions works randomly and generates by every run a different (within the statistics) set of particles for identical Twiss parameters. Although the MedAustron gantry is limited to protons only, the

TABLE I. Twiss parameters in the gantry nozzle including the beam scattering calculated by WinAGILE. The numbers are rounded to three decimal digits and represent the Twiss parameters at the exit of the given scattering element.

Position	The full ellipse			The bar		
	β (m)	α (1)	ε (π mm mrad)	β (m)	α (1)	ε (π mm mrad)
Gantry entrance	1.784	−0.536	1.000	39.776	−53.556	0.010
Al-foil no. 1	6.378	0.169	1.050	20.576	0.000	0.316
Hostaphan® no. 1	4.171	0.111	1.606	5.248	0.000	1.237
Al-foil no. 2	4.087	0.106	1.637	5.085	−0.001	1.277
Vacuum window	3.282	0.085	2.039	3.710	−0.001	1.750
Gantry isocenter	1.758	−0.500	4.925	1.808	−0.514	4.787

rotatorlike optics can be applied to carbon gantries, too. Figure 10 shows the emittance patterns of the carbon-ion beam at the outer side of the vacuum window [Fig. 10(a)] and at the gantry isocenter [Fig. 10(b)].

It can be seen that—in contrast to protons—beam scattering in the vacuum window is not enough to equalize the emittance patterns of the bar and the full ellipse. The area of the scattered bar (red) is still smaller than the area of the scattered full ellipse (blue) at the outer side of the vacuum window [plot 10(a)]. Nevertheless, with an additional scattering contribution from the DDS monitors and from the air gap to the patient, the emittance patterns are equalized at the gantry isocenter also for the carbon-ion beams [plot 10(b)]. It should be noted that the overall scattering for carbon ions is less than for protons, indeed [compare the plots 8(d) with 10(b)]. Nevertheless, there is still enough scattering to equalize the scattered emittance diagrams of the bar and the full ellipse at the gantry isocenter even for the top-energy carbon beam. This is a consequence of the flat orientation of the bar in the phase space at the inner side of the vacuum window, which is "a byproduct" of the beam waist at the gantry isocenter. Thus, for both particle species (protons and carbon ions) at top energies, equalized emittance patterns are obtained at the gantry isocenter.

D. Rotation-independent beam transport with scattering

Finally, to demonstrate the rotation-independent beam transport with scattering, which is a natural consequence of combining the rotation-independent optics with rotation-independent scattering, Fig. 11 presents the FWHM beam envelopes including beam scattering in the gantry nozzle. The envelopes are calculated for the gantry rotation angles from $\varphi = 0°$ to $\varphi = 90°$ with 15° steps. At the gantry rotation angle $\varphi = 0°$, the horizontal gantry plane transports the bar, and the vertical gantry plane transports the full ellipse (the red envelopes). At the gantry rotation angle $\varphi = 90°$, the situation is reversed (the blue envelopes). The beam envelopes at the intermediate angles are depicted as the solid black lines. The beam parameters at the fixed beamline exit correspond to Figs. 8 and 9.

E. The projected-average mode

An interesting, special, and useful situation comes with the gantry rotation angle 45°. Applying the coordinate system rotation transfer matrix (1) for this particular angle of 45° in the sigma-matrix transformation (7) yields

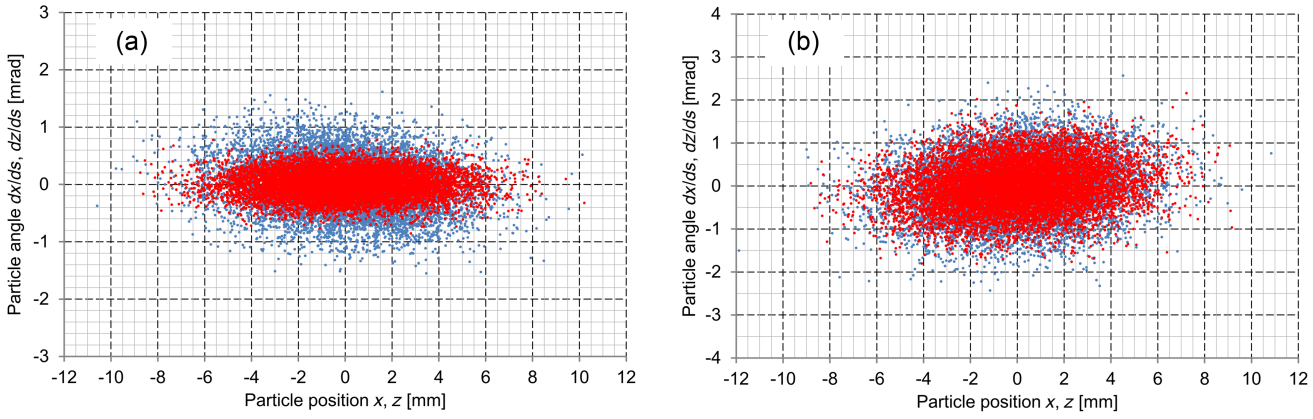

FIG. 10. Emittance diagrams of the full ellipse (blue) and the bar (red) including beam scattering in the gantry nozzle and in the air gap in front of the patient for a 400 MeV/n carbon-ion beam. (a) Outer side of the vacuum window and (b) gantry isocenter.

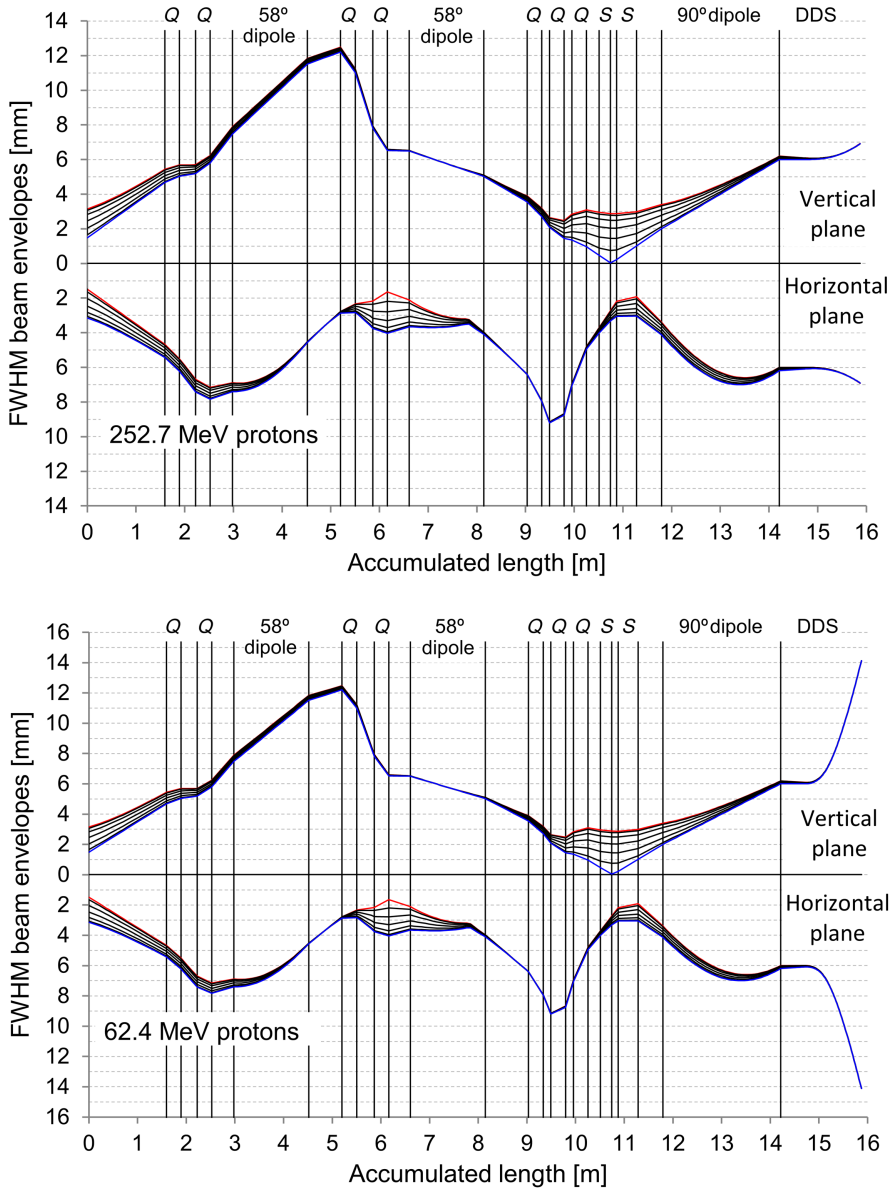

FIG. 11. FWHM beam envelopes in the parallel-to-point gantry with magnification 3 m for the rotatorlike gantry optics including beam scattering in the gantry nozzle for 252.7 MeV protons (top panel) and 62.4 MeV protons (bottom panel) at different angles of gantry rotation. Input beam parameters are identical to the input beam parameters in Figs. 8 and 9. Red lines: gantry rotation angle $\varphi = 0°$, blue lines: gantry rotation angle $\varphi = 90°$, black lines: gantry rotation angles $\varphi = 15°$, $\varphi = 30°$, $\varphi = 45°$, $\varphi = 60°$, and $\varphi = 75°$. Vertical lines: position of the main gantry elements (Q, quadrupoles and S, scanning magnets). DDS: dose delivery system. Upper half of the plot: the vertical gantry plane and lower half of the plot: the horizontal gantry plane.

$$\boldsymbol{\sigma}_{45°} = \frac{1}{2}\begin{pmatrix} (\sigma_{11}+\sigma_{33}) & (\sigma_{12}+\sigma_{34}) & (\sigma_{33}-\sigma_{11}) & (\sigma_{34}-\sigma_{12}) \\ (\sigma_{12}+\sigma_{34}) & (\sigma_{22}+\sigma_{44}) & (\sigma_{34}-\sigma_{12}) & (\sigma_{44}-\sigma_{22}) \\ (\sigma_{33}-\sigma_{11}) & (\sigma_{34}-\sigma_{12}) & (\sigma_{11}+\sigma_{33}) & (\sigma_{12}+\sigma_{34}) \\ (\sigma_{34}-\sigma_{12}) & (\sigma_{44}-\sigma_{22}) & (\sigma_{12}+\sigma_{34}) & (\sigma_{22}+\sigma_{44}) \end{pmatrix}, \tag{47}$$

where $\boldsymbol{\sigma}_{45°}$ is the beam sigma matrix as seen by the gantry entrance in the gantry local coordinate system. The σ_{ij} terms are defined by Eq. (2) and it is essential to point out that the beam at the fixed beamline exit is assumed to be free from the horizontal-to-vertical coupling. It can be seen that the horizontal beam sigma submatrix becomes

identical to the vertical one, both representing the arithmetic mean of the original horizontal and vertical beam sigma-matrix terms without any constraints regarding the symmetry/asymmetry of the incoming beam. Let us call this arithmetic mean the "projected" average. Also the bar and the full ellipse (strictly speaking their projections including the beam profiles) become identical at the gantry entrance at the gantry rotation angle 45°. This is also the reason why the 2D-emittance diagrams of the bar and the full ellipse must meet at 45° as mentioned in Sec. VI B.

The projected average mode can be used to verify correctness of the gantry transfer matrix. Because this mode guarantees the same horizontal and vertical sigma submatrices at the gantry entrance, the horizontal and vertical beam sizes at the gantry isocenter must be the same for identical horizontal and vertical gantry magnification. Otherwise, the magnifications are not correct.

Finally, let us mention another interesting property of the rotatorlike gantry optics. The rotatorlike gantry—like any other rotator—rotates the beam spot at the isocenter by the gantry rotation angle. This makes it possible to make sure that the beam spot is really round and free from horizontal-to-vertical coupling in the real space. Such a beam-roundness check can be done by measuring the horizontal and vertical beam-spot profiles at different gantry angles. Because the beam monitors in the gantry nozzle always measure the beam-spot profile in the gantry horizontal and vertical planes, rotating the beam spot in the local gantry coordinate system provides beam-spot profiles at different directions across the beam spot.

F. Last remarks

The last remark concerns all presented beam envelopes in the horizontal gantry plane. They are calculated taking into account also a contribution from the beam momentum spread in the dispersive regions of the gantry. The relative momentum spread of 0.11% was assumed. The dispersion contribution is added linearly to the momentum-spread free envelope, which is the model implemented in WinAGILE. This is the reason why the beam size does not drop to (almost) zero in the horizontal plane even when the bar is standing upright in the phase space if there is a nonzero dispersion. This is different from the nonbending vertical gantry plane where zero dispersion is assumed.

VII. CONCLUSIONS

A novel so-called rotatorlike ion-optical concept for rotating gantries has been invented and introduced in this paper. It combines two ion-optical matching principles—the sigma matching and the rotator matching—directly into the first-order gantry transfer matrix. A sigma-matching gantry becomes a rotator. The concept is based on theoretical calculations that expand the sigma-matching principle to the beam covariances at the gantry isocenter. Together with a special constraint for the phase-advance difference between the two gantry transverse planes, a rotatorlike transfer matrix can be gained.

The feasibility of this concept has been verified on the MedAustron proton gantry that represents rather typical configuration of an isocentric barrel upstream-scanning gantry. Both regimes—the point-to-point as well as the parallel-to-point imaging—are possible. The parallel-to-point mode showed more favorable (smaller) beam envelopes inside the gantry compared to the point-to-point one. Using the rotatorlike gantry optics is the most effective matching technique since it combines advantages of the sigma matching with unique ion-optical properties of the rotator. The latter guarantees that the beam scattering in the gantry nozzle always starts from the same emittance pattern on the inner surface of the vacuum window of the last gantry dipole independently from the gantry rotation angle. This makes it possible to simplify and to optimize the design of the gantry optics and the gantry nozzle for scattered beams. Finally, we have shown that the vacuum window can act as the dedicated scattering foil used for the scattering-foil matching. As demonstrated in Fig. 8, combination of the rotatorlike gantry optics with scattering in the gantry nozzle unifies entirely the emittance diagrams of the bar and the full ellipse at the gantry isocenter. The rotatorlike gantry optics makes it possible to form beam waists at the gantry isocenter (in both gantry transverse planes simultaneously) that are independent from the gantry rotation angle. This provides flat orientation of the bar in the phase space at the vacuum window, that is independent from the gantry rotation angle, too. Such an orientation guarantees the most effective scattering of the bar and, consequently, the most effective and "rapid" balancing of the two transverse beam emittance patterns at the gantry isocenter. Neither an extra dedicated scattering foil nor an external rotator is needed upstream of the gantry. We have shown that this technique works for both particle species (protons and carbon ions) at the top energies used for cancer treatment (≈250 MeV and ≈400 MeV/n, respectively).

ACKNOWLEDGMENTS

M. P. and Slovak University of Technology in Bratislava acknowledge and appreciate the funding from the European Union's Horizon 2020 Research and Innovation Program under the GA No. 101004730. Starting from year 2024, the work has been co-funded also by the Slovak Scientific Grant Agency under the Grant No. VEGA 1/0010/24.

[1] L. Badano, M. Benedikt, P. Bryant, M. Crescenti, P. Holy, P. Knaus, A. Maier, M. Pullia, and S. Rossi, Synchrotrons for hadron therapy: Part I, Nucl. Instrum. Methods Phys. Res., Sect. A **430**, 512 (1999).

[2] M. Benedikt, P. Bryant, and M. Pullia, A new concept for the control of a slow-extracted beam in a line with rotational optics: Part II, Nucl. Instrum. Methods Phys. Res., Sect. A **430**, 523 (1999).

[3] M. Benedikt, Optics design of the extraction lines for the MedAustron hadron therapy centre, Nucl. Instrum. Methods Phys. Res., Sect. A **539**, 25 (2005).

[4] R. Taylor, E. Benedetto, M. Sapinski, and J. Pasternak, Slow extraction modelling for NIMMS hadron therapy synchrotrons, J. Phys. Conf. Ser. **2420**, 012101 (2023).

[5] T. Haberer, W. Becher, D. Schardt, and G. Kraft, Magnetic scanning system for heavy-ion therapy, Nucl. Instrum. Methods Phys. Res., Sect. A **330**, 296 (1993).

[6] W. T. Chu, B. A. Ludewigt, and T. R. Renner, Instrumentation for treatment of cancer using proton and light-ion beams, Rev. Sci. Instrum. **64**, 2055 (1993).

[7] J. Janik and M. Muller, Some remarks on the ion optics of beam delivery systems for tumor treatment, Nucl. Instrum. Methods Phys. Res., Sect. A **84**, 117 (1994).

[8] M. Pavlovic, Beam-optics study of the gantry beam delivery system for light-ion cancer therapy, Nucl. Instrum. Methods Phys. Res., Sect. A **399**, 439 (1997).

[9] S. Dong, F. Zhang, N. Schlegel, W. Wang, J. Sun, Y. Sheng, and X. Xia, The influence of beam optics asymmetric distribution on dose in scanning carbon-ion radiotherapy, J. Appl. Clin. Med. Phys. **23**, e13656 (2022).

[10] J. Y. Tang, L. Liu, Z. Yang, S. X. Fang, and X. L. Guan, Emittance balancing technique for the resonant slow extraction from a synchrotron, Phys. Rev. ST Accel. Beams **12**, 050101 (2009).

[11] Takuji Furukawa and Koji Noda, Compensation of the asymmetric phase-space distribution for a slowly extracted beam from a synchrotron, Nucl. Instrum. Methods Phys. Res., Sect. A **565**, 430 (2006).

[12] Y. Iwata, K. Noda, T. Murakami, T. Shirai, T. Furukawa, T. Fujita, S. Mori, K. Mizushima, K. Shouda, T. Fujimoto, T. Ogitsu, T. Obana, N. Amemiya, T. Orikasa, S. Takami, and S. Takayama, Development of a superconducting rotating-gantry for heavy-ion therapy, Nucl. Instrum. Methods Phys. Res., Sect. A **317**, 793 (2013).

[13] Y. Iwata, K. Noda, T. Shirai, T. Murakami, T. Furukawa, S. Mori, T. Fujita, A. Itano, K. Shouda, K. Mizushima, T. Fujimoto, T. Ogitsu, T. Obana, N. Amemiya, T. Orikasa, S. Takami, S. Takayama, and I. Watanabe, Design of a superconducting rotating gantry for heavy-ion therapy, Phys. Rev. ST Accel. Beams **15**, 044701 (2012).

[14] Y. Iwata, T. Fujimoto, S. Matsuba, T. Fujita, S. Sato, T. Furukawa, Y. Hara, K. Mizushima, Y. Saraya, R. Tansho, N. Saotome, T. Shirai, and K. Noda, Beam commissioning of a superconducting rotating-gantry for carbon-ion radiotherapy, Nucl. Instrum. Methods Phys. Res., Sect. A **834**, 71 (2016).

[15] Y. Iwata, T. Fujimoto, S. Matsuba, T. Fujita, S. Sato, T. Furukawa, Y. Hara, K. Mizushima, Y. Saraya, R. Tansho, N. Saotome, T. Shirai, and K. Noda, Recent progress of a superconducting rotating-gantry for carbon-ion radiotherapy, Nucl. Instrum. Methods Phys. Res., Sect. A **406**, 338 (2017).

[16] M. Benedikt, P. Bryant, P. Holy, and M. Pullia, 'Riesenrad' ion gantry for hadrontherapy: Part III, Nucl. Instrum. Methods Phys. Res., Sect. A **430**, 534 (1999).

[17] S. A. Reimoser and M. Pavlovic, Engineering design and study of the beam position accuracy in the "Riesenrad" ion gantry, Nucl. Instrum. Methods Phys. Res., Sect. A **456**, 390 (2001).

[18] M. Benedikt and C. Carli, Optical design of a beam delivery system using a rotator, CERN, Geneva, Switzerland, Technical Report No. CERN/PS 96-41-DI, 1996.

[19] L. C. Teng (private communication).

[20] E. Griesmayer, T. Schreiner, and M. Pavlovic, The MedAustron project, Nucl. Instrum. Methods Phys. Res., Sect. A **258**, 134 (2007).

[21] M. T. F. Pivi, L. Adler, G. Guidoboni, G. Kowarik, C. Kurfürst, C. Maderböck, M. Pavlovič, D. A. Prokopovich, M. G. Pullia, V. Rizzoglio, and I. Strašík, Commissioning of a gantry beamline with rotator at a synchrotron-based ion therapy center, Phys. Rev. Accel. Beams **27**, 023503 (2024).

[22] M. Pavlovic, A design of a rotating gantry for non-symmetric ion-therapy beams, Nucl. Instrum. Methods Phys. Res., Sect. A **438**, 548 (1999).

[23] M. Pavlovic, E. Griesmayer, and R. Seemann, Beam-transport study of an isocentric rotating ion gantry with minimum number of quadrupoles, Nucl. Instrum. Methods Phys. Res., Sect. A **545**, 412 (2005).

[24] H. Owen, A. Lomax, and S. Jolly, Current and future accelerator technologies for charged particle therapy, Nucl. Instrum. Methods Phys. Res., Sect. A **809**, 96 (2016).

[25] E. W. Collings, L. C. Lu, N. Gupta, and M. D. Sumption, Accelerators, gantries, magnets and imaging systems for particle beam therapy: Recent status and prospects for improvement, Front. Oncol. **11**, 737837 (2022).

[26] H. Owen, R. MacKay, K. Peach, and S. Smith, Hadron accelerators for radiotherapy, Contemp. Phys. **55**, 55 (2014).

[27] H. Owen, D. Holder, J. R. Alonso, and R. Mackay, Technologies for delivery of proton and ion beams for radiotherapy, Int. J. Mod. Phys. A **29**, 1441002 (2014).

[28] J. R. Alonso and T. A. Antaya, Superconductivity in medicine, in *Reviews of Accelerator Science and Technology volume 5: Applications of Superconducting Technology to Accelerator*, edited by A. W. Chao and W. Chou (World Scientific, Singapore, 2012), pp. 227–263, 10.1142/S1793626812300095.

[29] E. Felcini, G. Frisella, A. Mereghetti, M. G. Pullia, S. Savazzi, M. T. F. Pivi, and E. Benedetto, Beam optics studies for a novel gantry for hadron therapy, J. Phys. Conf. Ser. **2420**, 012098 (2023).

[30] M. G. Pullia *et al.*, Explorative studies of an innovative superconducting gantry, J. Phys. Conf. Ser. **2420**, 012099 (2023).

[31] E. Pedroni, D. Meer, C. Bula, S. Safai, and S. Zenklusen, Pencil beam characteristics of the next-generation proton scanning gantry of PSI: Design issues and initial commissioning results, Eur. Phys. J. Plus **126**, 66 (2011).

[32] E. Pedroni, R. Bearpark, T. Böhringer, A. Coray, J. Duppich, S. Forss, D. George, M. Grossmann, G. Goitein, C. Hilbes, M. Jermann, L. Shixiong, A. Lomax, M. Negrazus, M. Schippers, and G. Kotrle, The PSI Gantry

2: A second generation proton scanning gantry, Z. Med. Phys. **14**, 25 (2004).

[33] H. Wiedemann, *Particle Accelerator Physics: Basic Principles and Linear Beam Dynamics* (Springer-Verlag, Berlin, Heidelberg, 1993), ISBN 3-540-56550-7, 0-387-56550-7, p. 445.

[34] M. Pavlovic, J. Bokor, and A. Šagátová, Rotators for matching non-symmetric ion-therapy beams to rotating gantries, Int. J. Mod. Phys. Conf. Ser. **44**, 1660220 (2016).

[35] J. Bokor and M. Pavlovic, An ion-optical design study of a carbon-ion rotating gantry with a superconducting final bending magnet, Nucl. Instrum. Methods Phys. Res., Sect. A **812**, 122 (2016).

[36] P. Bryant, AGILE, a tool for interactive lattice design, edited by W. A. Mitaroff, C. Petit-Jean-Genaz, J. Poole, M. Regler, and J. L. Laclare, in *Proceedings of the 7th European Particle Accelerator Conference, EPAC-2000, Vienna, Austria* (EPS, Geneva, 2000), pp. 1357–1359, https://accelconf.web.cern.ch/e00/PAPERS/TUP6B03.pdf.

[37] http://cern.ch/madx/

[38] https://fluka.cern/

[39] M. Palm, M. Benedikt, and U. Dorda, Transfer line scattering model of therapeutic hadron beams and applications to nozzle and gantry optimization, Phys. Rev. ST Accel. Beams **16**, 014702 (2013)..

[40] M. Palm, M. Benedikt, and U. Dorda, Erratum: Transfer line scattering model of therapeutic hadron beams and applications to nozzle and gantry optimization, Phys. Rev. ST Accel. Beams **16**, 014702 (2013); Phys. Rev. ST Accel. Beams**16**, 039901 (2013).